J. Fluid Mech. (1986), *vol.* 163, *pp.* 365–391
Printed in Great Britain

Assessment of local isotropy using measurements in a turbulent plane jet

By R. A. ANTONIA, F. ANSELMET AND A. J. CHAMBERS
Department of Mechanical Engineering, University of Newcastle, N.S.W., 2308, Australia

(Received 3 October 1984 and in revised form 21 June 1985)

Following a review of the difficulties associated with the measurement and interpretation of statistics of the small-scale motion, the evidence for and against local isotropy is assessed in the light of measurements in a turbulent plane jet at moderate values of the Reynolds and Péclet numbers. These measurements include spatial derivatives with respect to different spatial directions of the longitudinal velocity fluctuation and of the temperature fluctuation. Relations between mean-square values of these derivatives suggest strong departures from local isotropy for both velocity and temperature. In contrast, the locally isotropic forms of the vorticity and temperature dissipation budgets are approximately satisfied. Possible contamination of the fine-scale measurements by the anisotropic large-scale motion is assessed in the context of the measured structure functions of temperature and of the measured skewness of the streamwise derivative of temperature. Structure functions are, within the framework of local isotropy, consistent with the average frequency and amplitude of temperature signatures that characterize the quasi-organized large-scale motion. Conditional averages associated with this motion account, in an approximate way, for the skewness of the temperature derivative but make negligible contributions to the skewness of velocity derivatives. The degree of spatial organization of the fine structure is inferred from conditional statistics of temperature derivatives.

1. Introduction

The concept of local isotropy is important to the theory of turbulence since its validity implies a certain universality of the small-scale motion or fine structure. From a practical point of view, the importance of the concept cannot be overemphasized since its use leads to a significant simplification of expressions for $\bar{\epsilon}$ and $\bar{\epsilon}_\theta$, respectively the average dissipations for the turbulent kinetic energy and half the temperature variance. Since Kolmogorov's (1941*a*) local-similarity theory, the increase in the intermittency of the fine structure with an increase in the turbulent Reynolds number R_λ has received a great deal of attention, both experimentally and theoretically (e.g. chapter 8 of Monin & Yaglom 1975). Although the expectation of local isotropy is strictly associated with sufficiently large, preferably atmospheric, values of R_λ and of the turbulent Péclet number Pe, several statistics of small-scale turbulence at atmospheric Reynolds number have, apparently, not indicated a decrease in the departure from local isotropy (e.g. Gibson, Friehe & McConnell 1977). This trend suggests an obvious but important question: Why and how does anisotropy, which is observed at laboratory Reynolds numbers, persist at atmospheric Reynolds numbers? Progress in answering this question has been hampered by the ambiguity in interpreting the fine-scale measurements in the context of isotropy.

Source	References
(*a*) Inadequate spatial resolution of sensors	Corrections for velocity: Wyngaard (1968, 1969); Schedvin, Stegen & Gibson (1974) Corrections for temperature: Wyngaard (1971*a*)
(*b*) Non-convergence of tails of p.d.f.s	Tennekes & Wyngaard (1972); Frenkiel & Klebanoff (1975)
(*c*) Non-convergence of tails of spectra	Champagne (1978)
(*d*) Inadequate averaging time	Tennekes & Wyngaard (1972); Antonia *et al.* (1982)
(*e*) Poor signal/noise ratio	Tennekes & Wyngaard (1972)
(*f*) Inadequate choice of cutoff frequency of low-pass filter	Kuo & Corrsin (1971); Champagne (1978); Gagne & Hopfinger (1979); Antonia *et al.* (1982)
(*g*) Choice of appropriate convection velocity	Corrections to Taylor's hypothesis: velocity – Lumley (1965); Heskestad (1965); temperature – Wyngaard & Clifford (1977); Champagne *et al.* (1977)
(*h*) Errors associated with the use of parallel (hot or cold) wires	Wyngaard (1969); Mestayer & Chambaud (1969); Tavoularis & Corrsin (1981); Brown *et al.* (1983*a*, *b*); Antonia *et al.* (1984, 1985)

TABLE 1. Possible sources of error in fine-scale measurements

Possible factors that have contributed to this ambiguity are (not necessarily in order of importance):

(i) uncertainties in measured statistics of velocity and temperature derivatives;

(ii) the different sensitivities of various tests of local isotropy;

(iii) difficulties in devising appropriate guidelines for comparing velocity and temperature fields;

(iv) the likely contamination of the fine structure by the relatively organized and anisotropic large-scale motion.

Each of these factors is briefly discussed below.

(i) *Possible sources of systematic error in measurements.* Most of these are well known and are listed in table 1 with appropriate references. We concentrate here on (*g*) since the verification of Taylor's hypothesis (e.g. $u_{1,1} \equiv (-\bar{U}_1)^{-1} u_{1,t}$, where $\bar{U}_1$ is the mean velocity in the x_1 direction, $u_{1,1} \equiv \partial u_1/\partial x_1$ and $u_{1,t} \equiv \partial u_1/\partial t$) is implicit in most local isotropy tests that are available in the literature. Corrections to this hypothesis were developed by Lumley (1965) and Heskestad (1965) to account for the effect of a fluctuating velocity field and have, for example, been applied by Champagne (1978) to fine-scale velocity measurements. Corrections analogous to those of Lumley and Heskestad were proposed by Wyngaard & Clifford (1977) and Champagne *et al.* (1977) for the temperature field. Antonia, Phan-Thien & Chambers (1980) calculated the probability density function (p.d.f.) of temporal velocity and temperature derivatives for two choices of the fluctuating convection velocity and an assumed Gaussian p.d.f. of the spatial derivatives. The calculations led to corrections that were in the opposite direction to those that were proposed on the basis of the equations of motion but with the use of a number of untested assumptions. Antonia *et al.* (1980) noted in

particular that the assumed independence between small and large scales needed verification.

A more direct approach, although not without complications, for assessing Taylor's hypothesis is to measure the streamwise spatial derivative simultaneously with the temporal derivative. This approach is feasible in the case of temperature derivatives. Browne, Antonia & Rajagopalan (1983*a*) found that both p.d.f.s and spectra of $\theta_{,1}$, obtained on the centreline of a plane jet, were in reasonable agreement with those of either $\overline{U}_1^{-1}\theta_{,t}$ or $U_1^{-1}\theta_{,t}$. Also p.d.f.s and spectra of spatial temperature increments, for separations extending to about 13η (η is the Kolmogorov lengthscale $\nu^{\frac{3}{4}}/\bar{\epsilon}^{\frac{1}{4}}$), were in reasonable agreement with those for temporal temperature increments when Taylor's hypothesis was used. Browne *et al.* (1983*a*) used the isotropic value of $\bar{\epsilon}$, viz $\bar{\epsilon} = 15\nu\overline{u_{1,1}^2}$, to estimate η. Although the use of isotropy may seem prejudicial, it is unlikely, in view of the exponent of $\bar{\epsilon}$ in the relation $\eta = \nu^{\frac{3}{4}}/\bar{\epsilon}^{\frac{1}{4}}$, that the estimate of η was in error. It is also possible that $\bar{\epsilon} \approx 15\nu\overline{u_{1,1}^2}$ may be a reasonable approximation despite the fact that individual terms of $\bar{\epsilon}$ do not satisfy isotropy.

Although the result of Browne *et al.* was obtained only at the jet centreline and needs to be extended to other positions in the flow (as well as to other flows), we have preferred for the present work to lean towards the experimental evidence, limited as it may be, rather than the available, theoretically based, corrections. Consequently, we have used Taylor's hypothesis consistently in the present paper.

In the light of table 1, the prospect of obtaining accurate fine-scale measurements may seem rather daunting. In this context, it is pertinent to note that the possibility of using numerical simulations (e.g. Kerr 1985), albeit at small Reynolds numbers, for comparison with fine-scale measurements seems promising.

(ii) *Local isotropy tests with different degrees of sensitivity.* Tests can take the form of relationships between moments of velocity of temperature derivatives, relationships between spectra of different velocity or temperature derivatives, or between structure functions of velocity or temperature. Tests can also be applied at different levels in the sense that attention may be focused on a particular range of lengthscales or a particular range of frequencies. For example, a second-order derivative would give more weight to the higher-wavenumber end of the spectrum than the first-order derivative. Tests involving spectra or structure functions can be applied in the inertial range, if such a range exists, or in the viscous range or in both these ranges. Bradshaw (1967, 1969) suggested that the existence of an inertial subrange in turbulent flow may be compatible with the hypothesis of second-class† isotropy and that this hypothesis provides a useful way of determining $\bar{\epsilon}$ at least for sufficiently large Reynolds numbers (e.g. Lawn 1971). Champagne, Harris & Corrsin (1970) concluded that the Kolmogorov '$-\frac{5}{3}$' law, even with proper component spectral magnitudes, is a relatively insensitive indicator of local isotropy. A similar sentiment was expressed, in slightly stronger terms, by Mestayer (1982). It should also be noted that different 'order' tests exist. For the velocity field, relationships between spectra of different velocity components may be thought to represent a test at the lowest order. A higher-order test would involve the spectral relationship between derivatives in the three spatial directions of the longitudinal velocity component. Note also that the spectral relationship between the three derivatives of the temperature fluctuation has been described as a 'second-order' test (Van Atta 1977*a*). It is clear from the

† The term 'second-class isotropy', as coined by Bradshaw (1967), implies a relaxation of the full requirements of local isotropy in that intensity spectra may satisfy local isotropy even though the shear-stress and heat-flux spectra do not.

previous remarks that many tests are available for testing local isotropy and that an appropriate choice is unlikely to be straightforward. Pragmatically, the appropriate test should perhaps fit the particular application: for example, when considering the budget of the temperature variance, it would help to know the magnitude of the departure from isotropy of the mean-square temperature derivatives.

(iii) *Guidelines for velocity vs temperature.* A direct comparison between velocity and temperature fields is not straightforward in view of the respective vector and scalar natures of these fields. A related difficulty is that of defining appropriate turbulent Reynolds and Péclet numbers. The use of $(\overline{u_1^2})^{\frac{1}{2}}$ and of the Taylor microscales λ_{u_1} and λ_θ in the definitions of $R_\lambda\,(\equiv (\overline{u_1^2})^{\frac{1}{2}}\lambda_{u_1}/\nu)$ and $Pe\,(\equiv (\overline{u_1^2})^{\frac{1}{2}}\lambda_\theta/\alpha$, α is the thermal diffusivity) may be ambiguous when departures from isotropy are known to occur. Corrsin (1963) suggested that it would be more prudent to use an r.m.s. resultant velocity fluctuation and some sort of averaged microscale instead of $(\overline{u_1^2})^{\frac{1}{2}}$ and λ_{u_1}. Fulachier & Antonia (1983) also noted that the use of the fluctuating-velocity vector may provide a more meaningful comparison between turbulent Reynolds and Péclet numbers.

In the absence of clear guidelines on how to compare fine-scale velocity and temperature fields appropriately, conclusions on the relative degree of isotropy of these fields can only be tentative. If it is argued that velocity is a forcing term in the transport equation for temperature, the anisotropy of the velocity field may be thought to influence the fine-scale temperature field. Mathematically, the comparison of relationships between mean-square velocity derivatives with those between mean-square temperature derivatives seem tenuous, since squared velocity derivatives are elements of tensors of rank 4 whereas squared temperature derivatives are elements of tensors of rank 2. Experimentally, considerable similarity may be observed between, for example, spectra of spatial derivatives $u_{1,1}$ or $u_{1,2}$ of velocity (Antonia, Browne & Chambers 1984) with corresponding spectra $\theta_{,1}$ or $\theta_{,2}$ for temperature (Antonia, Browne & Chambers 1985).

In the light of the above comments and the remarks made in (ii), it is difficult to interpret claims in the literature that the fine-scale velocity field satisfies isotropy over a wider range of scales than the temperature. Mestayer (1982) concluded that in a relatively high R_λ (≈ 600) laboratory boundary layer, local isotropy for the velocity field extended to about 20η compared with only about 3η for the temperature field. Mestayer, Choller & Lesieur (1984) speculated that this difference may be consistent with the apparently different Reynolds-number evolutions of 'bumps' in velocity and temperature spectra at the high-wavenumber end of the inertial range, noting that semi-local interactions between different wavenumbers are more effective for temperature than velocity. Although this speculation may be reasonable, Mestayer's (1982) conclusion can only be assessed properly when the degree of sensitivity of the tests that he applied can be appraised objectively.

Although, as noted earlier, the existence of an inertial range may be, at best, only a moderate indicator of local isotropy, it is of interest to comment on the relative degrees of scatter in the inertial-range constants for velocity and temperature. In a comprehensive review of published values for these constants, Yaglom (1981) found that the Kolmogorov constant for velocity shows significantly less scatter than the temperature constant. There is a possible explanation for the apparent disarray in reported values of the temperature constant. Accurate estimates of the inertial-range constants require an accurate estimate of $\bar{\epsilon}_\theta$. A significant number of estimates of the inertial-range constants has been based on isotropic values of $\bar{\epsilon}$ and $\bar{\epsilon}_\theta$. Although no rigorous experimental support is available, it is possible that the value $15\nu\overline{u_{1,1}^2}$ may be a reasonable approximation for $\bar{\epsilon}$. However, this does not necessarily imply that

the individual components of $\bar{\epsilon}$ satisfy local isotropy. On the contrary, there is evidence (e.g. Wygnanski & Fiedler 1969) to suggest that the ratios $\overline{u_{2,1}^2}/2\overline{u_{1,1}^2}$ and $\overline{u_{1,2}^2}/2\overline{u_{1,1}^2}$ are smaller and greater respectively than the isotropic value of unity. There may thus be sufficient compensation between different components of $\bar{\epsilon}$ to validate the isotropic approximation for $\bar{\epsilon}$. In contrast, there is a large amount of data, obtained in different shear flows, indicating that the ratios $\overline{\theta_{,2}^2}/\overline{\theta_{,1}^2}$ and $\overline{\theta_{,3}^2}/\overline{\theta_{,1}^2}$ are both greater than unity. There is consequently no compensation in the full expression for $\bar{\epsilon}_\theta$ and isotropic values of $\bar{\epsilon}_\theta$ may seriously underestimate the average temperature dissipation.†

(iv) *Contamination by the large structure.* The possibility that fine-scale measurements are contaminated by the anisotropy of the large-scale motion in non-homogeneous shear flows has been investigated by Gibson *et al.* (1977) and Sreenivasan, Antonia & Britz (1979). It would clearly be of interest to compare small-scale measurements in different non-homogeneous flows, preferably at the same R_λ, with different degrees of organization of the large-scale motion. A comparison with measurements in nearly homogeneous or nearly isotropic turbulence, where no organized motion is expected, should also be useful.

In view of all the above factors, but perhaps more specifically because of (i) and (iv), the need to document departures from local isotropy at laboratory values of R_λ seems important. The advantages of working in the atmosphere are well known: a large inertial range is possible and spatial resolution is not usually a problem since the Kolmogorov length η is of the order of 1 mm. A major disadvantage is that one forfeits control over experimental conditions and general experimental difficulties cannot be overlooked (e.g. C. A. Friehe 1983, private communication). It may also be more difficult to estimate effect (iv) accurately in the atmosphere than in the laboratory. Nelkin & Nakano (1984) stressed the importance of studying departures from local isotropy in the laboratory. Tavoularis & Corrsin (1981) provided this documentation with respect to moments of velocity and temperature derivatives in a quasi-homogeneous turbulent flow ($R_\lambda \approx 260$) with constant mean-velocity and -temperature gradients. In the present paper we document, by paying particular attention to (i) and (iv), departures from isotropy for the fine-scale velocity and temperature fields in the self-preserving region of a turbulent plane jet. The accuracy of the fine-scale measurements is discussed in §2 and results for high-order moments of first-order derivatives of u_1 and θ are compared in §3 with those of Tavoularis & Corrsin (1981). Mean-square values of second-order derivatives are considered separately in §4 by using isotropic forms of the equations for the turbulent vorticity budget and the temperature dissipation. In §5, several models for the possible contamination of the fine structure by the anisotropic large structure are assessed. The spatial organization of the fine structure is examined in §6 using conditional averages of an approximation to the temperature dissipation. We also attempt to discuss this organization in terms of the known topology of the flow.

2. Experimental details and accuracy of moments

A description of the jet facility and general instrumentation is given in Antonia *et al.* (1983*a*). We briefly recall here the experimental configurations and conditions that are relevant to the present measurements. The jet issues from a nozzle of width $d = 12.7$ mm and height 25 cm at a nominal jet exit velocity $\overline{U}_j$ of 9 m/s

† A good estimate of $\bar{\epsilon}_\theta$ can, in principle, be obtained as the difference in the budget of the temperature variance. Such an approach requires, however, that all other terms in the budget are obtained accurately.

($\overline{U}_j d/\nu \approx 7550$). All measurements were made at a distance x_1 of $40d$ from the nozzle after establishing that the flow was approximately self-preserving at $x_1 = 20d$. On the centreline ($x_2 = 0$), $\overline{U}_1 \equiv U_0 \approx 3.4$ m/s, $(\overline{u_1^2})^{\frac{1}{2}}/U_0 \approx 0.2$ and $R_\lambda \approx 160$. For most measurements, the jet was heated at a nominal nozzle-exit temperature $\overline{T}_j$ of 25 °C above ambient. At $x_2 = 0$, the local mean temperature T_0 (at $x_2 = 0$) was about 9 °C above ambient, $(\overline{\theta^2})^{\frac{1}{2}}/T_0 \approx 0.16$ and $Pe \approx 94$. The amount of heat used was sufficiently small for temperature to be considered a passive marker of the flow. Quantities such as the Reynolds shear stress were the same with as without heating, indicating that the dynamics of the flow were not influenced by the temperature field. The Kolmogorov microscale η was about 0.14 mm at $x_2 = 0$. The corresponding Kolmogorov frequency $f_K = U_0/2\pi\eta$ was approximately 3.8 kHz. The half-widths L_u and L_θ, derived from mean-velocity and mean-temperature profiles respectively, were 0.6 m and 0.073 m.

The results given in the next section are based on several types of measurements:

(i) Two parallel hot wires (Pt–10 % Rh) were aligned in the x_3 or spanwise direction and separated in the x_2 or main shear direction. Each wire had a diameter of 1.3 μm and a length of 0.17 mm and was operated with a DISA 55M01 constant-temperature anemometer at a resistance ratio of 1.8. The separation $\Delta\hat{x}_2 \equiv \Delta x_2/\eta$ (hereinafter the circumflex will denote normalization by η) between the wires was varied in the range 1.4–10. The flow was not heated for these measurements.

(ii) Two parallel cold wires (0.63 μm, Pt–10 % Rh) were aligned in the x_3 direction and spaced in either the x_1 or x_2 direction. The wires were operated with a constant-current system supplying 0.1 mA to each wire. Wire lengths of 0.41 mm and 0.32 mm were used. For the x_1 separation (a detailed description of the experimental arrangement is given in Browne *et al.* 1983*a*) the longer wire was placed upstream to avoid any possible interference with the other wire. For the x_2 separation, the longer wire was fixed at $x_2 = 0$ and the shorter wire traversed in the positive x_2 direction. The ranges of separation used were approximately 0.71η–14η and 0.93η–12.3η in the x_1 and x_2 directions respectively.

(iii) Two parallel cold wires, each of length ≈ 0.6 mm, were aligned in the x_2 direction, separated by a distance of 0.65 mm in the x_3 direction and centrally located in a rake of cold wires. All wires in the rake were at the same x_1 and x_2 but at different x_3 locations. The rake was moved to different values of x_2. A total of eight wires, including the parallel-wire pair, was used. Each wire (0.63 μm, Pt–10 % Rh) was operated at a current of 0.1 mA. The rake covered a spanwise separation of $0.9L_u$.

(iv) A spanwise rake of cold wires was also used with an X-wire/cold-wire arrangement replacing the parallel wires in the centre of the rake. The X-wires (5 μm, Pt–10 % Rh) were operated at an overheat of 0.8 with constant-temperature anemometers. The cold wire (0.63 μm, Pt–10 % Rh) was located about 0.5 mm upstream of the X-wires and operated in a constant-current (0.1 mA) circuit. The rake covered a spanwise separation of $1.06L_u$.

(v) Measurements at $x_2 = 0$ of u_1 and θ. Two wires, one hot (Pt, 2.5 μm, 0.37 mm length) and one cold (Pt–10 % Rh, 0.63 μm, 0.32 mm length) were aligned in the x_3 direction and separated in the x_2 direction by about 0.5 mm.

Signals from the hot or cold wires were first recorded on an eight-channel FM tape recorder at 381 mm/s and subsequently digitized on a PDP 11/34 computer. For the majority of experiments, the hot-wire signals were digitized at a sampling frequency f_s of 7 kHz after low-pass filtering at a cutoff frequency f_c of 3.5 kHz. To determine f_c, signals proportional to $u_{1,1}$ and $u_{1,2}$ were obtained, with the hot wires at the exit plane of the jet, using an analog differentiator and an analog computer. Spectra

of these signals were obtained with a real-time spectrum analyser. These 'noise' spectra were stored and compared with the 'signal' spectra obtained with the wires at $x_1/d = 40$. The frequency f_c (≈ 3.5 kHz) was identified with that at which the signal could no longer be clearly distinguished from the noise. A similar procedure was used on analog signals proportional to $\theta_{,1}$ and $\theta_{,2}$ to determine the cutoff frequency for temperature. In this case, f_c was about 3.7 kHz and temperature or temperature-derivative signals were digitized at a sampling frequency of 7.4 kHz. Signal-to-noise ratios for $\theta_{,1}$ and $\theta_{,2}$ were about 18 and 22 dB respectively, while corresponding ratios for $u_{1,1}$ and $u_{1,2}$ were almost equal (≈ 24 dB).

Although it would have been desirable to set f_c at a somewhat larger value than the Kolmogorov frequency f_K, the present value of f_c ($\approx f_K$), dictated by signal/noise considerations, was estimated to be satisfactory for the present study. Antonia, Satyaprakash & Hussain (1982) estimated that the optimum setting for f_c was about $1.75 f_K$ on the basis of data for $u_{1,1}$ obtained on the centreline of plane and circular jets. However, the variation in statistics of $u_{1,1}$ was relatively small once f_c exceeded f_K; for example, the flatness factor of $u_{1,1}$, the highest-order moment of interest here, increased by about 7% in the range $1 \leqslant f_c/f_K \leqslant 1.75$. We also ascertained that the convergence of the tails of the present $u_{1,1}$ and $\theta_{,1}$ spectra was good. Although spectral closure for the derivatives of $u_{1,1}$ and $\theta_{,1}$ was not complete (see §4), this discrepancy was not sufficiently large to affect the conclusions of §4.

The analog signals $u_{1,1}$ and $u_{1,2}$ were not digitized; the actual hot-wire voltages were digitized and linearized on the computer. Time derivatives and differences of these linearized signals were formed on the computer. The analog signals $\theta_{,1}$ and $\theta_{,2}$ were digitized along with the original cold-wire voltages from which they were derived. Statistics of $\theta_{,1}$ and $\theta_{,2}$ formed on the computer were in close agreement with those for the analog derivatives.

There are many sources of error associated with the use of parallel wires for obtaining spatial derivatives. We briefly recall some of these (more details can be found in the references listed in table 1).

(*a*) *Possible differences in the time constants of the parallel wires and possible mismatch between frequency responses of the parallel measuring paths.* The parallel cold wires used for measurements of types (ii) and (iii) had approximately the same time constant (-3 dB frequency was estimated to be 4.8 kHz, ± 5%). The effect of the prong–wire interaction (Paranthoen, Petit & Lecordier 1982) on the low-frequency response of cold wires can be significant, especially when the length-to-diameter ratio decreases below about 1000. However, this effect is more likely to be important for temperature variance or flux measurements than for measurements which weight the high-frequency end of the spectrum, and corrections for this effect were not applied to the present data. Possible phase shifts between the parallel signal paths for both hot- and cold-wire measurements, including wires, cables, anemometers and filters, were not detected in cross-spectra of signals obtained for small separations between the wires.

(*b*) *Spatial-resolution limitations.* These may be especially severe for measurements with parallel wires. As the distance between the wires decreases, the spatial resolution is expected to increase but this advantage is offset by the relatively large systematic errors that occur at small separations due to relatively small errors in static calibration. To avoid this latter difficulty, the separations between the wires should be increased but the attenuation in the high-frequency components of the signals must then be taken into account. A possible correction for the effect of separation on the difference between temperature or velocity signals was outlined by Antonia

et al. (1984, 1985). Their procedure consisted of extrapolating various statistics of these differences to zero separation, ignoring in this extrapolation data obtained at small separations. Spatial-resolution effects can also be caused by inadequate wire lengths. Corrections for hot and cold wires (table 1) were not applied since, for the majority of the present fine-scale measurements, the wire lengths were typically in the range 1.2η to 3η.

(*c*) *Effect of velocity sensitivity of cold wires on temperature statistics.* For the present experimental conditions, the velocity sensitivity for a 0.63 μm cold wire of length $\approx 3\eta$ was approximately 10^{-2} °C s/m and $\overline{\theta^2_{,1}}$ was underestimated by about 0.15%. A calculation, similar to that of Wyngaard (1971*b*), indicated that the contribution to the measured skewness of $\theta_{,1}$, due to the velocity sensitivity of the cold wire, is about 4.5×10^{-3}. This estimate is negligible in comparison with the measured skewness (table 2) which is of order one.

Two important checks of the accuracy of high-order moments of derivatives or structure functions relate to the adequacy of integration times and the convergence of the tails of the p.d.f.s (table 1). For the present measurements, the duration of the digital records was in the range 60–120 s. Running moments of derivatives of u_1 and θ were examined to estimate the times required for these moments to converge to within $\pm 5\%$ of their final values. For $n = 4$, the highest order considered here, these times were comfortably smaller than the total record durations. Approximate convergence times for $\overline{\theta^4_{,1}}$, $\overline{\theta^4_{,2}}$, $\overline{u^4_{1,1}}$ and $\overline{u^4_{1,2}}$ were 30%, 50%, 40% and 70% respectively of the total record duration.

P.d.f.s of $u_{1,1}$, $u_{1,2}$, $\theta_{,1}$ and $\theta_{,2}$ are shown in figure 1 on a semi-log plot to emphasize the tails of the p.d.f. p. The notation is such that, for example,

$$\int_{-\infty}^{\infty} p(\theta^*_{,1})\,\mathrm{d}\gamma = 1,$$

where γ represents values in probability space assumed by the physical variable $\theta_{,1}$ and the asterisk means that $\theta_{,1}$ is centred and normalized by its r.m.s. value. The p.d.f.s for $u_{1,2}$ and $\theta_{,2}$ were formed for $\Delta\hat{x}_2 \approx 5$, a separation which is large enough to avoid the systematic calibration errors (e.g. Mestayer & Chambaud 1979) but not sufficiently small to ignore the effect of spectral attenuation at large wavenumbers (e.g. Wyngaard 1969; Browne *et al.* 1983*a*). A correction for this latter effect will be considered later in this section. The p.d.f.s of temperature derivatives peak near $\gamma = 0$ and spread to larger values of $|\gamma|$ than velocity-derivative p.d.f.s.† There is no significant difference between p.d.f.s of streamwise and lateral derivatives, for either velocity or temperature. The uncertainty of the magnitude of p at large values of $|\gamma|$ is indicated in figure 1 by error bars. To check convergence of the tails, integrands $\gamma^n p$ were plotted in terms of γ. We limit ourselves to showing only distributions for $n = 4$, the highest order considered. While the integrands in figure 2 show satisfactory closure, this closure is better for positive than negative values of γ, in the case of $u_{1,2}$ or $\theta_{,2}$. Symmetry with respect to $\gamma = 0$ of $|\gamma^n|p$ is better approximated by the p.d.f.s of the x_2 than the x_1 derivatives. Satisfactory closure of the integrands corresponding to second-order derivatives, with respect to x_1, of velocity and temperature is demonstrated in figure 3. These derivatives appear in the budgets (§4) for vorticity and temperature dissipation.

† Similar differences can be observed in Anselmet's (1983) measured p.d.f.s of temperature-structure functions of u_1 and θ on the axis of a jet.

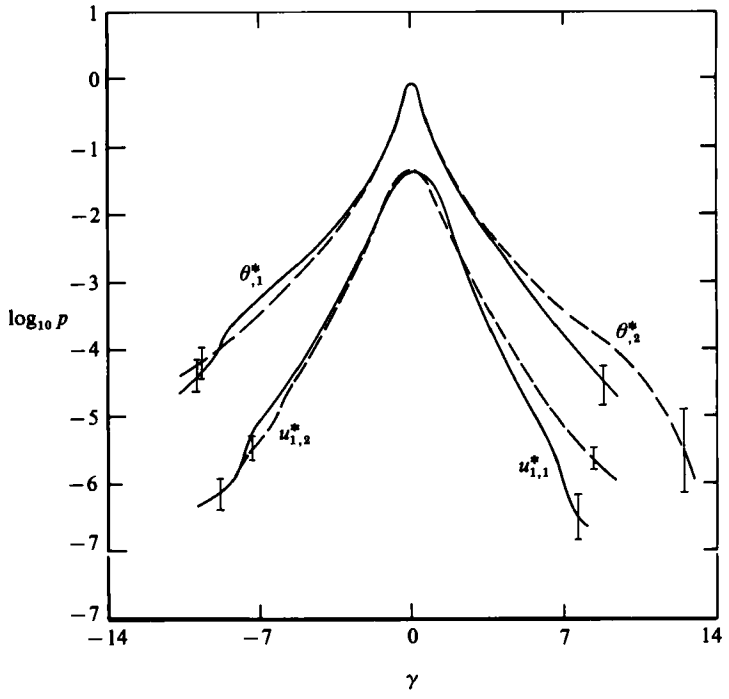

FIGURE 1. Probability density functions of velocity and temperature derivatives at $x_2 = 0$. Upper curves: ——, $p(\theta^*_{,1})$; — —, $p(\theta^*_{,2})$. Lower curves: ——, $p(u^*_{1,1})$; — —, $p(u^*_{1,2})$.

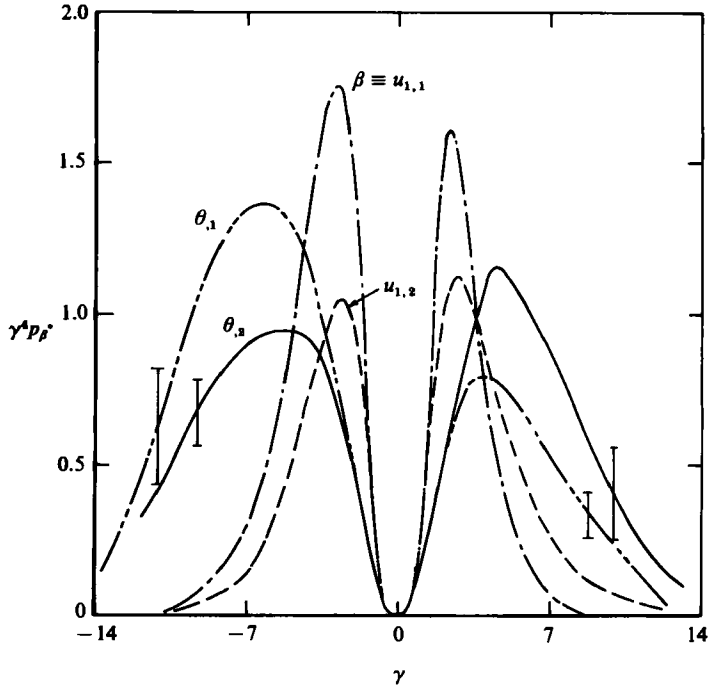

FIGURE 2. Integrands corresponding to fourth-order moments of velocity and temperature derivatives at $x_2 = 0$: — — —, $\gamma^4 p(u^*_{1,1})$; — —, $\gamma^4 p(u^*_{1,2})$; — — — —, $\gamma^4 p(\theta^*_{,1})$; ——, $\gamma^4 p(\theta^*_{,2})$.

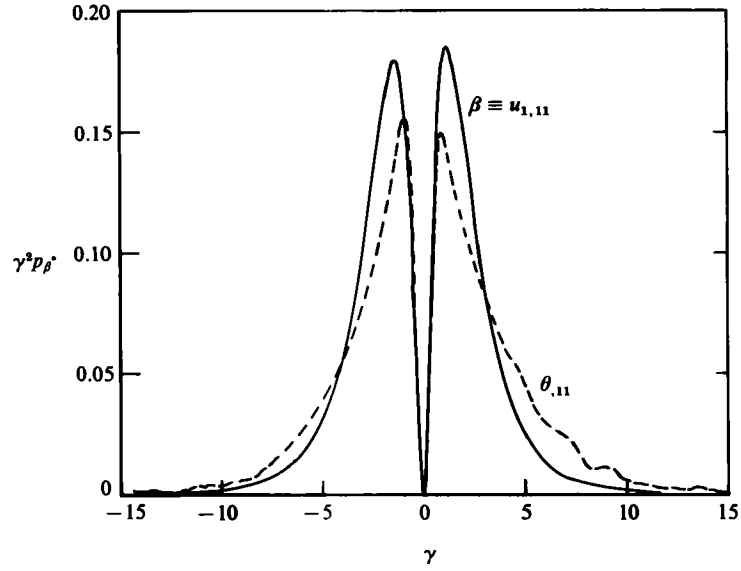

FIGURE 3. Integrands corresponding to second-order moments of second derivatives of velocity and temperature derivatives at $x_2 = 0$. ——, $\gamma^2 p(u^*_{1,11})$; — —, $\gamma^2 p(\theta^*_{,11})$.

3. Moments of velocity and temperature derivatives

Moments, up to order 4, of derivatives of u_1 and θ are presented in table 2 at the centreline ($x_2 = 0$) of the jet. Also shown in table 2 are the corresponding moments measured by Tavoularis & Corrsin (1981) in a significantly different flow, a quasi-homogeneous turbulent shear flow with constant values of $\overline{U}_{1,2}$ and $\overline{T}_{,2}$, but for slightly larger values of R_λ and Pe than in the present flow. Before comparing the results in the two flows, it is appropriate to point out how derivatives with respect to x_2 were corrected for the effect of separation Δx_2 between the wires. For example, to determine the flatness factor $F_{\theta,2}$ ($\equiv \overline{\theta^4_{,2}}/(\overline{\theta^2_{,2}})^2$) the correct or non-attenuated digital values of $\overline{\theta^4_{,2}}$ and $(\overline{\theta^2_{,2}})^2$ were first obtained prior to forming their ratio. To determine $\theta^2_{,2}$, Antonia *et al.* (1984) extrapolated measurements of $\overline{(\Delta\theta/\Delta x_2)^2}$, obtained for $\Delta\hat{x}_2$ in the range 5–11, to $\Delta\hat{x}_2 = 0$. A linear extrapolation was used as a first approximation; a more appropriate extrapolation, based on theoretical calculations developed by Wyngaard (1969) and Browne *et al.* (1983*a*), requires a knowledge of the correct spectrum of velocity or temperature and was not implemented. The procedure adopted by Antonia *et al.* (1984) was followed here for $\overline{\theta^4_{,2}}$, as shown in figure 4. The corrected value of $F_{\theta,2}$, shown as a solid line in figure 4, is 13 % smaller than the approximately constant values of the ratio $\overline{(\Delta\theta/\Delta x_2)^4}/(\overline{(\Delta\theta/\Delta x_2)^2})^2$ over the range $\Delta\hat{x}_2 \lesssim 5$. All normalized moments (including correlations between different derivatives) in table 2, which include $\theta_{,2}$ or $u_{1,2}$, were corrected using a similar procedure to that adopted for correcting $F_{\theta,2}$.

Tavoularis & Corrsin (1981) measured $\Delta\theta/\Delta x_2$ using parallel wires of lengths 2.26η and 4.52η, the derivative $\theta_{,2}$ being obtained by extrapolating to $\Delta\hat{x}_2 = 0$ values corresponding to separations in the range $3.4 \lesssim \Delta\hat{x}_2 \lesssim 11.3$. Data corresponding to values of $\Delta\hat{x}_2$ as small as 3.4, the minimum separation considered in the experiment, were included in the extrapolation but details of the extrapolation are not given in the paper. Measurements of $\Delta u_1/\Delta x_2$ were made of wires of length 7η and a separation

	Present (plane jet) $x_2 = 0$	Isotropic value	Tavoularis & Corrsin (quasi-homogeneous shear flow)
R_λ	≈ 160	—	≈ 260
Pe	94	—	118
$\overline{u_{1,2}^2}/2\overline{u_{1,1}^2}$	1.8	1	2.2
$S_{u_{1,2}} \equiv \overline{u_{1,2}^3}/(\overline{u_{1,2}^2})^{\frac{3}{2}}$	−0.04	0	0.62
$S_{u_{1,1}}$	−0.43	−0.44†	−0.42
$F_{u_{1,2}} \equiv \overline{u_{1,2}^4}/(\overline{u_{1,2}^2})^2$	4.9	—	7.3
$F_{u_{1,1}}$	5.8	—	6.5
$\overline{u_{1,1}u_{1,2}}/(\overline{u_{1,1}^2})^{\frac{1}{2}}(\overline{u_{1,2}^2})^{\frac{1}{2}}$	0.23	0	−0.44
$\overline{\theta_{,2}^2}/\overline{\theta_{,1}^2}$	2	1	1.82
$S_{\theta,2}$	≈ 0	0	1.1
$S_{\theta,1}$	−0.85	0	−0.95
$F_{\theta,2}$	12.5	—	11.0
$F_{\theta,1}$	16.1	—	15.0
$\overline{\theta_{,1}\theta_{,2}}/(\overline{\theta_{,1}^2})^{\frac{1}{2}}(\overline{\theta_{,2}^2})^{\frac{1}{2}}$	−0.13	0	−0.48

† From isotropic vorticity budget, (4).

TABLE 2. Comparison of moments of velocity and temperature derivatives with data of Tavoularis & Corrsin (1981)

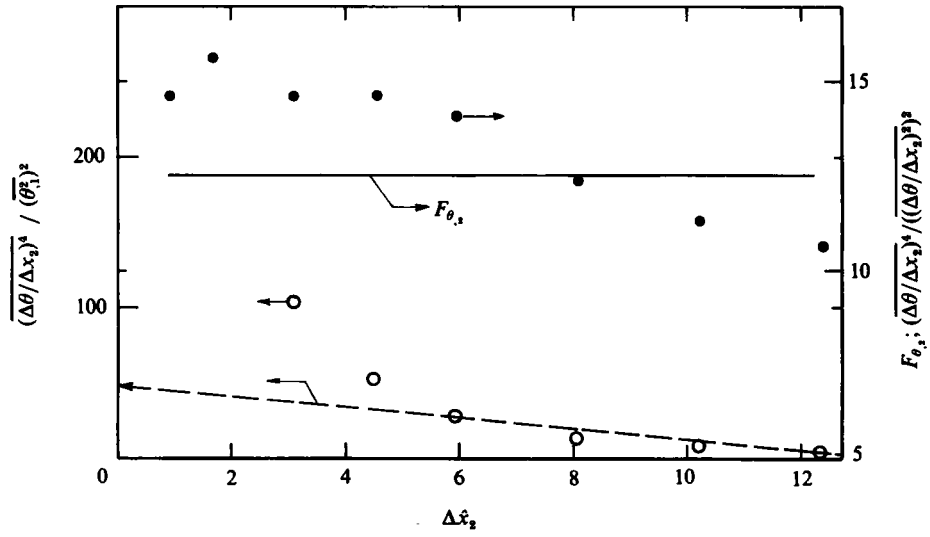

FIGURE 4. Dependence of separation $\Delta\hat{x}_2$ of normalized and non-normalized fourth-order moments of $(\Delta\theta/\Delta x_2)$ at $x_2 = 0$. ○, $\overline{(\Delta\theta/\Delta x_2)^4}/(\overline{\theta_{,1}^2})^2$ [measured]; — —, linear extrapolation to $\Delta\hat{x}_2 = 0$ of measurements for $\Delta\hat{x}_2 \gtrsim 5$. ●, $\overline{(\Delta\theta/\Delta x_2)^4}/(\overline{(\Delta\theta/\Delta x_2)^2})^2$ [measured]; ——, $F_{\theta,2}$ derived from extrapolations of $\overline{(\Delta\theta/\Delta x_2)^4}$ and $\overline{(\Delta\theta/\Delta x_2)^2}$.

$\Delta\hat{x}_2 \approx 2.8$. These data were corrected for wire-length effects but the authors do not indicate whether they were corrected for the separation between wires.

The comparison in table 2 indicates points of agreement but also several 'apparent' differences between moments in the two flows. Directional analogies, noted by Tavoularis & Corrsin, between the fine structures of velocity and temperature, also apply to the present data. For example, the inequalities ($\overline{u_{1,2}^2} > 2\overline{u_{1,1}^2}$;† $\overline{\theta_{,2}^2} > \overline{\theta_{,1}^2}$) are of the same order in these two flows.‡. Allowing for the small differences in R_λ and Pe, there is reasonable agreement in the case of the skewness $S_{u_{1,1}} \equiv \overline{u_{1,1}^3}/(\overline{u_{1,1}^2})^{\frac{3}{2}}$ and $S_{\theta_{,1}}$ and flatness factors $F_{u_{1,1}} \equiv \overline{u_{1,1}^4}/(\overline{u_{1,1}^2})^2$ and $F_{\theta_{,1}}$. The ratio $F_{\theta_{,1}}/F_{\theta_{,2}}$ is about the same (≈ 1.3) in both flows, compared with an isotropic value of unity. The standard deviation associated with the present value of $S_{u_{1,1}}$ was calculated to be ± 0.017 using ten separate estimates of the skewness. For $S_{\theta_{,1}}$, $F_{\theta_{,1}}$, $F_{u_{1,1}}$ the standard deviations were ± 0.038, ± 0.61 and ± 0.095 respectively. The major differences in table 2 occur in quantities involving $u_{1,2}$ or $\theta_{,2}$ where they are raised to an odd power. The present nearly zero values for $S_{u_{1,2}}$ and $S_{\theta_{,2}}$ reflect the symmetry constraint on the centreline. This constraint also requires that the correlations $\overline{u_{1,1}u_{1,2}}$ and $\overline{\theta_{,1}\theta_{,2}}$ are zero.§ Their measured values are not quite zero, the departure from zero being more significant in the case of $\overline{u_{1,1}u_{1,2}}$ than $\overline{\theta_{,1}\theta_{,2}}$. Estimated uncertainties in $\overline{u_{1,1}u_{1,2}}/(\overline{u_{1,1}^2})^{\frac{1}{2}}(\overline{u_{1,2}^2})^{\frac{1}{2}}$ and $\overline{\theta_{,1}\theta_{,2}}/(\overline{\theta_{,1}^2})^{\frac{1}{2}}(\overline{\theta_{,2}^2})^{\frac{1}{2}}$, due to the effect of Δx_2, are ± 0.04 and ± 0.05 respectively. We do not have an explanation for the non-zero value of $\overline{u_{1,1}u_{1,2}}$; although the fixed wire was correctly located at the centreline, the moving wire was traversed in only the positive x_2 direction. Unfortunately, the hot-wire pair was not traversed across the jet.

It may be argued that Tavoularis & Corrsin's non-zero values of moments which involve odd powers of $x_{1,2}$ and $\theta_{,2}$ reflect the non-zero magnitudes of mean-velocity and -temperature gradients. Tavoularis & Corrsin explained the signs of their observed values of $S_{u_{1,2}}$ and $S_{\theta_{,2}}$ with the use of a mixing-length-type model. Specifically, they suggested

$$\operatorname{sgn} S_{u_{1,2}} = \operatorname{sgn} \overline{U}_{1,2} \tag{1}$$

and

$$\operatorname{sgn} S_{\theta_{,2}} = \operatorname{sgn} \overline{U}_{1,2} \operatorname{sgn} \overline{T}_{,2}. \tag{2}$$

The skewness $S_{\theta_{,2}}$ has an opposite sign to $S_{\theta_{,1}}$, Sreenivasan & Tavoularis (1980) having earlier shown that

$$\operatorname{sgn} S_{\theta_{,1}} = -\operatorname{sgn} \overline{U}_{1,2} \operatorname{sgn} \overline{T}_{,2}.\P \tag{3}$$

Tavoularis & Corrsin indicated that (2) is compatible with the boundary-layer data of Sreenivasan, Antonia & Danh (1977). Further, the magnitude of $S_{\theta_{,2}}$ is nearly the same in these two flows although the measurements of Sreenivasan *et al.* showed little variation of $S_{\theta_{,2}}$ in the logarithmic region, across which there are significant variations in $\overline{U}_{1,2}$ (40–160 s^{-1}) and $\overline{T}_{,2}$ (70–280 °C m^{-1}). In Tavoularis & Corrsin's flow, $\overline{U}_{1,2} = 46.8\ \mathrm{s}^{-1}$ and $\overline{T}_{,2} = 9.5$ °C m^{-1}.

† Anisotropy is also reflected by the inequality between $\overline{u_{2,1}^2}$ and $2\overline{u_{2,1}^2}$ but, in this case, published measurements in the nearly self-preserving region of a plane jet indicate that $\overline{u_{2,1}^2} < 2\overline{u_{1,1}^2}$ (e.g. Gutmark & Wygnanski 1976; Everitt & Robins 1978; Antonia *et al.* 1983*a*).

‡ Similar inequalities have also been observed by Verollet (1977) in a boundary layer.

§ The present magnitude of $\overline{\theta_{,1}\theta_{,2}}/(\overline{\theta_{,1}^2})^{\frac{1}{2}}(\overline{\theta_{,2}^2})^{\frac{1}{2}}$ shown in figure 2 is smaller than that (≈ 0.3) reported by Antonia & Browne (1983) in the same flow. This latter value was not corrected for the effect of Δx_2.

¶ Budwig, Tavoularis & Corrsin (1985) have shown that the mean shear is not necessary for the development of a non-zero temperature-gradient skewness. They concluded that $\operatorname{sgn} S_{\theta_{,i}} = \operatorname{sgn} \overline{T}_{,i}$, with $i = 1$, 2 or 3.

Tavoularis & Corrsin estimated that $\overline{u_{1,1}\,u_{1,2}}/(\overline{u_{1,1}^2})^{\frac{1}{2}}(\overline{u_{1,2}^2})^{\frac{1}{2}}$ was about -0.44, using isocorrelation contours obtained by Harris, Graham & Corrsin (1977) in essentially the same flow but in the absence of a temperature gradient. Earlier measurements (Champagne, Harris & Corrsin 1970) in the same type of flow but with a smaller mean-velocity gradient ($\overline{U}_{1,2} \approx 12.9\ \mathrm{s}^{-1}$) yielded a value of -0.21. These results tend to imply that, at least in this flow, the effect of velocity gradient may influence statistics of the small-scale structure and suggested a need for a systematic study of the effects of $\overline{U}_{1,2}$ and $\overline{T}_{,2}$. In a non-homogeneous shear flow, the influence of $\overline{U}_{1,2}$ and $\overline{T}_{,2}$ may not be as important but this speculation needs to be confirmed. Differences that exist between the fine-structure statistics in the present flow and in the quasi-homogeneous shear flow may be, at least in part, related to differences in the large structure. The present non-homogeneous shear flow is characterized by the presence of a quasi-organized large-scale motion. There is no evidence for such organization in the quasi-homogeneous shear flow of Tavoularis & Corrsin.

On the basis of the relatively large values, measured in their flow, for $\overline{\theta_{,1}\,\theta_{,2}}/(\overline{\theta_{,1}^2})^{\frac{1}{2}}(\overline{\theta_{,2}^2})^{\frac{1}{2}}$ and $\overline{u_{1,1}\,u_{1,2}}/(\overline{u_{1,1}^2})^{\frac{1}{2}}(\overline{u_{1,2}^2})^{\frac{1}{2}}$ (see table 2), Tavoularis & Corrsin speculated that there is a high probability that large values of $(u_{1,1}, u_{1,2})$ and/or $(\theta_{,1}, \theta_{,2})$ occur simultaneously. Although the present values for the above correlation coefficients are small at $x_2 = 0$ (they should be zero by symmetry), joint probability-density functions (j.p.d.f.s) of $(u_{1,1}^2, u_{1,2}^2)$ or $(\theta_{,1}^2, \theta_{,2}^2)$ at $x_2 = 0$ (figure 5*b*) clearly indicate that large values of one of the quantities in these pairs is large when the other quantity is small. The notation used for figure 5 is consistent with that in figure 1, with γ and δ indicating values in probability space taken by the physical variables. While the information shown in figure 5(*b*) was only available at $x_2 = 0$, the j.p.d.f. of $(\theta_{,1}^2, \theta_{,3}^2)$ was measured in the range $0 \leqslant x_2/L_u \leqslant 1$. The results were similar to those of figure 5(*b*), viz large values of $\theta_{,1}^2$ corresponded to small values of $\theta_{,3}^2$ and *vice versa*. An important consequence of these results is that the instantaneous behaviour of ϵ_θ cannot be inferred solely on the basis of $\theta_{,1}^2$. Although there is considerable similarity between the j.p.d.f.s for squared velocity and temperature derivatives in figure 5(*b*), there is less similarity between the j.p.d.f.s of the non-squared derivatives shown in figure 5(*a*). The j.p.d.f. contours of $(u_{1,1}, u_{1,2})$ are nearly elliptical and tilted whereas the contours for $(\theta_{,1}, \theta_{,2})$ resemble parallelograms and are more nearly symmetrical with respect to either axis.

4. Isotropic budgets of vorticity and of $\overline{(\partial\theta/\partial x)^2}$

It is of interest to consider whether the isotropic forms of the equations for the mean-square vorticity and average temperature dissipation are satisfied in the present flow. For stationary isotropic turbulence at large Reynolds numbers, the mean-square-vorticity budget may be written as (e.g. Batchelor & Townsend 1947; Champagne 1978)

$$\overline{u_{1,1}^3} = -2\nu\,\overline{u_{1,11}^2}.\dagger \tag{4}$$

Measurements at $x_2 = 0$ of $\overline{u_{1,1}^3}$ and $\overline{u_{1,11}^2}$ yielded an average value for the ratio of left and right sides in (4) of 0.97 (± 0.04), the uncertainty representing an r.m.s. error estimated from 12 separate experiments. From measurements by Wyngaard & Tennekes (1970) of $\overline{u_{1,11}^2}$ obtained from the spectrum of u_1, and of the skewness of $u_{1,1}$, the ratio of left and right sides of (4) is 0.93 (± 0.07). These measurements were in a curved mixing layer with $R_\lambda \approx 200$.

† The isotropic form of the sixth-order tensor required to obtain (4) was derived by Wyngaard and is given in the appendix of Champagne's (1978) paper.

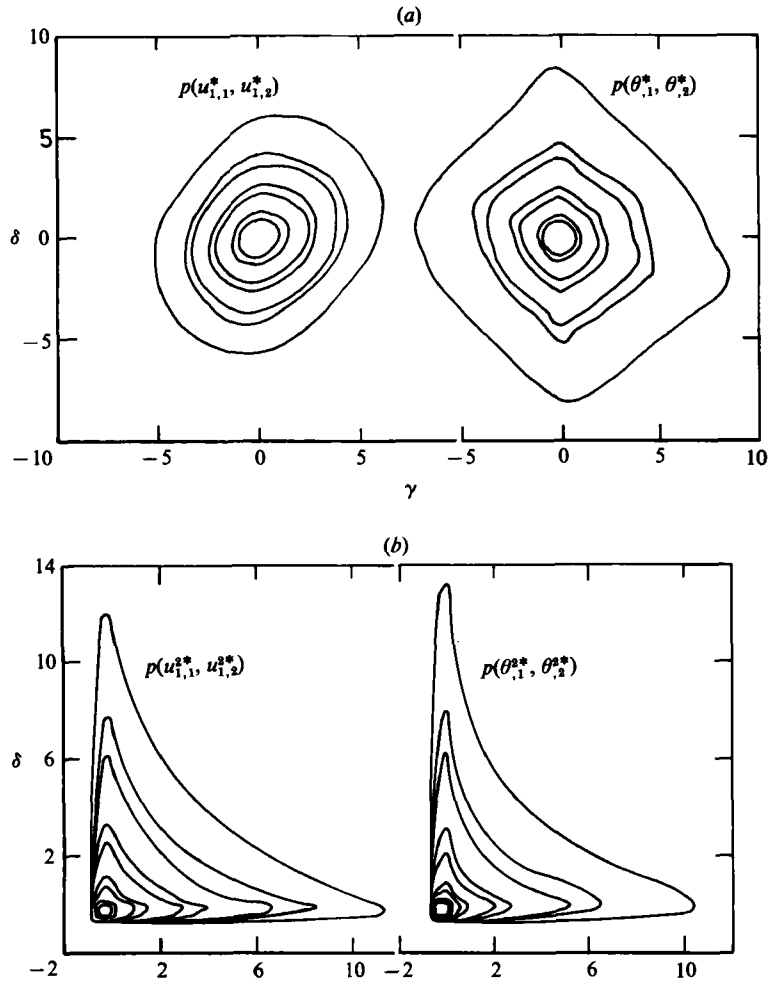

FIGURE 5. Contours of joint probability density functions between streamwise and lateral derivatives (and their squared values) of velocity or temperature at $x_2 = 0$. (*a*) $p(u^*_{1,1}, u^*_{1,2})$ (left) and $p(\theta^*_{,1}, \theta^*_{,2})$ (right). Magnitudes of outer-to-inner contours: 0.0001, 0.0005, 0.001, 0.005, 0.01, 0.05, 0.1. (*b*) $p(u^{2*}_{1,1}, u^{2*}_{1,2})$ (left) and $p(\theta^{2*}_{,1}, \theta^{2*}_{,2})$ (right). Magnitudes of outer-to-inner contours: 0.0001, 0.0005, 0.001, 0.005, 0.01, 0.05, 0.1, 0.5, 1.0.

The transport equation for the mean-square temperature gradient can be approximated, in large-Reynolds-number isotropic turbulence, by (e.g. Wyngaard 1971*b*)

$$\overline{u_{1,1}\theta^2_{,1}} = -\tfrac{2}{3}\alpha\overline{\theta^2_{,11}}. \tag{5}$$

The average ratio of measured values of left and right sides of (5) is 0.95 (± 0.05).

The reasonable agreement between experiment and the isotropic relations (4) and (5) may be thought of as surprising, given the moderately small value of R_λ in the present flow. Some insight into a possible explanation for this agreement may be gained by considering the spectral forms of relations (4) and (5). The spectral equivalent of (4) may be written as

$$\int_0^\infty Co_{u_{1,1}u^2_{1,1}}\,\mathrm{d}\hat{k}_1 = -2\times(15)^{\frac{3}{2}}\int_0^\infty \hat{k}_1^4\phi_{u_1}(\hat{k}_1)\,\mathrm{d}\hat{k}_1, \tag{6}$$

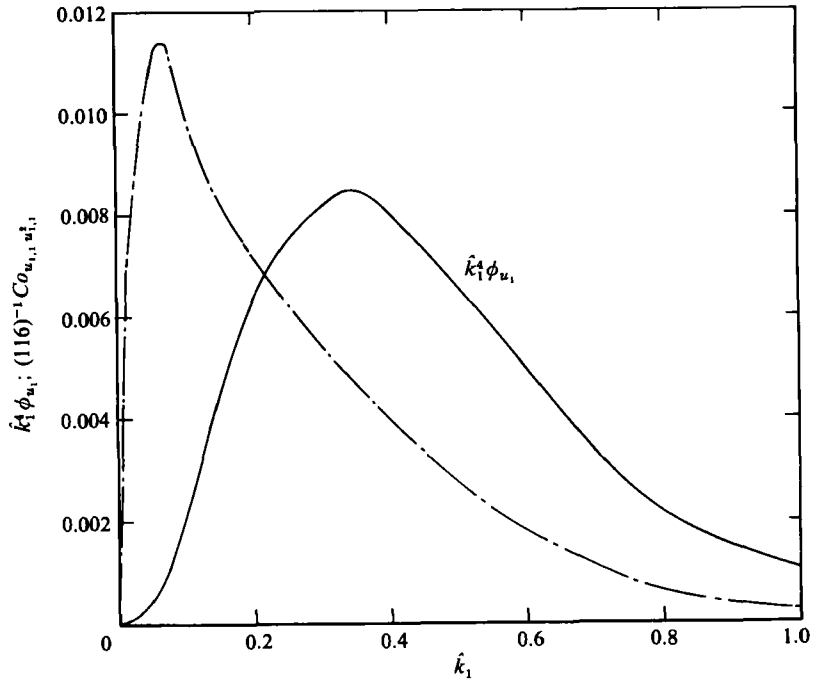

FIGURE 6. Production and dissipation terms in the isotropic form of the turbulent-vorticity equation at $x_2 = 0$. ——, dissipation $\hat{k}_1^4\phi_{u_1}$; — — —, production $(116)^{-1}\,Co_{u_{1,1}u_{1,1}^2}$.

where k_1 is the one-dimensional wavenumber and the cospectrum Co† between $u_{1,1}$ and $u_{1,1}^2$ is normalized such that the integral on the left side of (6) is equal to the skewness of $u_{1,1}$. The Kolmogorov normalized spectrum ϕ_{u_1} is defined such that

$$\int_0^\infty \phi_{u_1}(\hat{k}_1)\,\mathrm{d}\hat{k}_1 = \frac{\overline{u_1^2}}{U_\mathrm{K}^2},$$

where $U_\mathrm{K} \equiv (\nu\bar{\epsilon})^{\frac{1}{4}}$ is the Kolmogorov velocity scale. At $x_2 = 0$, $U_\mathrm{K} \approx 0.11$ m/s. The spectral equivalent of (5) is

$$\int_0^\infty Co_{u_{1,1}\theta_{,1}^2}\,\mathrm{d}\hat{k}_1 = -\frac{2\times(15)^{\frac{1}{2}}}{Pr^2}\int_0^\infty \hat{k}_1^4\phi_\theta(\hat{k}_1)\,\mathrm{d}\hat{k}_1, \tag{7}$$

where Pr is the molecular Prandtl number and the cospectrum between $u_{1,1}$ and $\theta_{,1}^2$ is normalized so that the integral on the left side of (7) is equal to the correlation coefficient $\overline{u_{1,1}\theta_{,1}^2}/[(\overline{u_{1,1}^2})^{\frac{1}{2}}\overline{\theta_{,1}^2}]$. The temperature spectrum is normalized so that

$$\int_0^\infty \phi_\theta(\hat{k}_1)\,\mathrm{d}\hat{k}_1 = \frac{\overline{\theta^2}}{\theta_\mathrm{K}^2},$$

where $\theta_\mathrm{K} \equiv (\bar{\epsilon}_\theta\,\eta/U_\mathrm{K})^{\frac{1}{2}}$ is the Kolmogorov temperature scale. At $x_2 = 0$, $\theta_\mathrm{K} \approx 0.17$ °C. This agreement is expected since it represents only a consistency check of the data. The non-zero values of $\hat{k}_1^4\phi_{u_1}$ (figure 6) and $\hat{k}_1^4\phi_\theta$ (figure 7) suggest that that the actual

† The interpretation of a cospectrum involving squared quantities is similar to that for non-squared quantities. For example, $Co_{u_{1,1}u_{1,1}^2}(\hat{k}_1)$ represents the correlation coefficient over a narrow wavenumber band centred on $\hat{k}_1$, of the quantities $u_{1,1}$ and $u_{1,1}^2$.

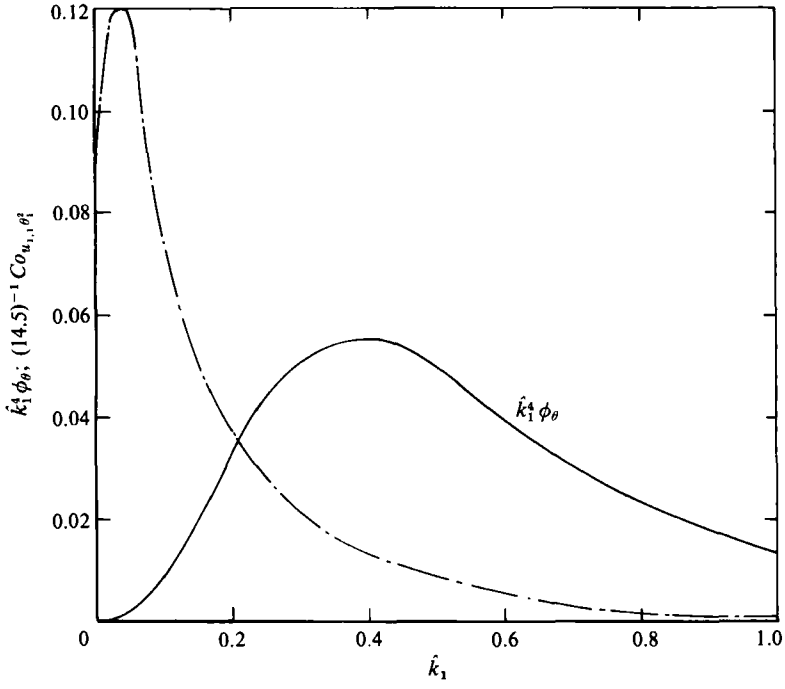

FIGURE 7. Production and dissipation terms in the isotropic form of the temperature-dissipation equation at $x_2 = 0$. ——, dissipation $\hat{k}_1^4 \phi_\theta$; — — —, production $(14.5)^{-1}\, Co_{u_{1,1}\theta_{,1}^2}$.

values of the ratios of left and right sides of (6) and (7) would be slightly smaller (but by no more than 10%) than those given above.

Distributions corresponding to left and right sides of (6) and (7) are shown in figures 6 and 8† respectively. The ratios of left and right sides of (6) and (7) are equal to 0.98 and 0.94 respectively, in reasonable agreement with the previous corresponding ratios in (4) and (5). The separation between the locations of the peaks in cospectra and dissipation is slightly larger for temperature (figure 7) than velocity (figure 6). It is noticeable, however, that the cospectrum between $u_{1,1}$ and $\theta_{,1}^2$ decays more rapidly with wavenumber than that between $u_{1,1}$ and $u_{1,1}^2$. For $\hat{k} > 0.3$ the area under the cospectrum in figure 7 represents only 13% of the total area whilst the area under the dissipation represents 82% of the total area. Corresponding values for figure 6 are 36% and 70%. A possible implication of figures 6 and 7 is that local isotropy is likely to be satisfied over a larger wavenumber range for temperature than for velocity since the cospectrum, which may be identified with the production term and a possible source of anisotropy, extends to larger wavenumbers for velocity than for temperature. This implication is consistent with the observation (Antonia *et al.* 1983*c*) that, in the present flow, Kolmogorov's (1941*b*) equation for the velocity structure functions is satisfied only for separations that fall inside the viscous range, whereas Yaglom's (1949) equation for temperature structure functions is satisfied for separations which extend up to the beginning of the inertial range. The inertial ranges, as inferred from second-order velocity and temperature structure functions, were estimated (Antonia *et al.* 1983*c*) to be $30 \lesssim r/\eta \lesssim 70$ and $20 \lesssim r/\eta \lesssim 50$ respectively.

† A slightly different form of the spectral contributions to the $\overline{\theta_{,1}^2}$ budget was plotted in the paper by Antonia & Browne (1983), where a more detailed discussion of the dissipation spectrum is given.

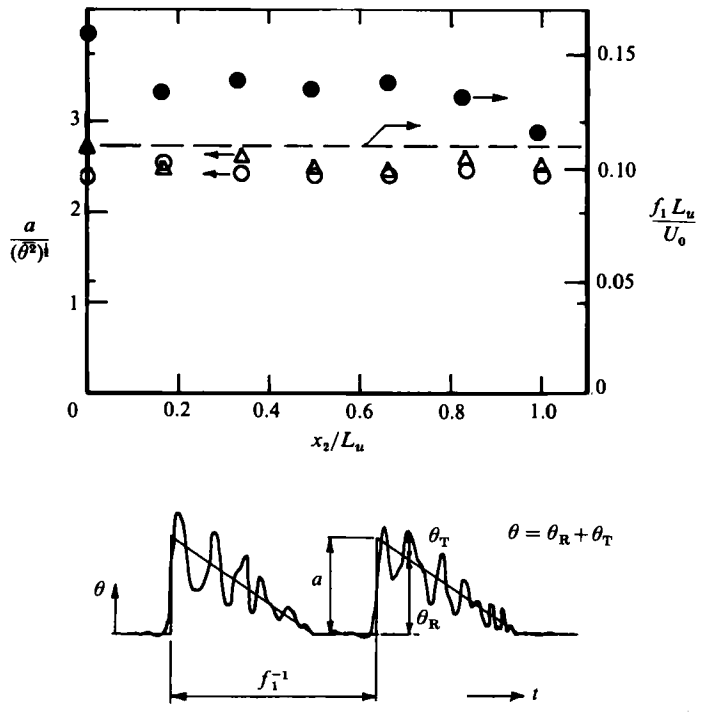

FIGURE 8. Average amplitude and frequency of temperature fronts. $a/(\overline{\theta^2})^{\frac{1}{2}}$: ○, using (9); △, using conditional averages of θ. $f_1 L_u/U_0$: ●, using (8) and (9); — —, Antonia *et al.* (1983*b*), Cervantes & Goldschmidt (1981).

5. Effect of large-scale motion on fine-scale statistics

The non-zero skewness of the temperature derivative or of the non-zero moments of odd-order temperature-structure functions need not be interpreted as indicating that the fine-scale temperature field is anisotropic (e.g. Sreenivasan *et al.* 1979; Antonia & Van Atta 1978; Subramanian & Antonia 1982). It is more reasonable to attribute the non-zero skewness to the anisotropy of the large-scale motion. Taylor (1958) was first to notice ramp-like temperature signatures in the atmospheric surface layer which were spatially coherent. Gibson *et al.* (1977) commented that such signatures appear to be a characteristic feature of scalar fields mixed by sheared turbulence. A physical interpretation of the ramp-like signatures in the context of the present flow is attempted in the next section, where the spatial organization of the flow is considered. It is of interest, however, to ascertain the extent to which a simple ramp-like model for temperature is consistent with measurements of both temperature and velocity derivatives.

Antonia & Van Atta (1978) used a relatively crude model of the ramp (shown in figure 8) whereby θ was assumed to be made up of a linear superposition of θ_R, a linear ramp of height a, and of random fluctuations θ_T with a characteristic timescale smaller than that of θ_R. With the assumption that $(\Delta\theta)_T$ is statistically independent of $(\Delta\theta)_R$, $\Delta\theta$ representing the temperature increment $\theta(t+\tau)-\theta(t)$, the average frequency f_1 of the ramps of structures is given by

$$f_1 = \frac{\overline{(\Delta\theta)^3}}{a^3 \tau} \tag{8}$$

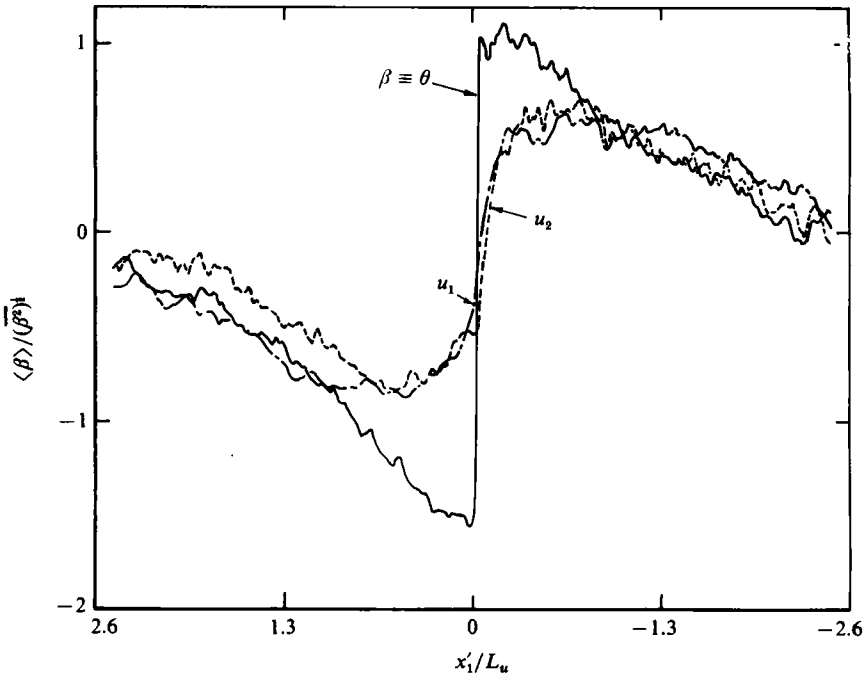

FIGURE 9. Conditional averages of u_1, u_2, θ at $x_2/L_u = 0.66$.

for inertial-range values of r. The magnitude of a can be obtained from a knowledge of second-, third- and fifth-order structure functions of temperature. For the present flow, the equation for a is given by (Antonia & Van Atta 1978)

$$a^3+\left(10\overline{(\Delta\theta)^2}-\frac{\overline{(\Delta\theta)^5}}{\overline{(\Delta\theta)^3}}\right)a-10\overline{(\Delta\theta)^3}=0. \tag{9}$$

From measurements of $\overline{(\Delta\theta)^n}$, with $n = 2, 3, 5$, values of a and f_1 were obtained, using (9) and (8), at different values of x_2. These values showed little variation over the range $20 \lesssim r\overline{U}_1/\eta \lesssim 80$ which encompasses the inertial ranges for velocity and temperature. There is practically no variation of $a/(\overline{\theta^2})^{\frac{1}{2}}$ with x_2, as shown in figure 8, this value comparing favourably with ramp amplitudes reported by Antonia & Van Atta (1978) for several non-homogeneous flows.

Temperature fronts, or spatially coherent sudden increases in θ, were identified using the rake of eight cold wires mentioned under (iii) in §2. The fronts were detected only when the increases could be visually identified on all temperature traces. Ensemble averages of θ, u_1 and u_2 were formed using the relation

$$\langle\beta(\tau_1)\rangle = N^{-1}\sum_{i=1}^{N}\beta(t_i+\tau_1), \tag{10}$$

where β stands for either θ, u_1 or u_2, t_i ($i = 1, \ldots, N$) are the detection instants, N is the total number of detections (typically 150–250) and the time τ_1 is measured from the instant of identification. Distributions of $\langle u_1\rangle$, $\langle u_2\rangle$, $\langle\theta\rangle$ at one value of x_2 are shown in figure 9 in terms of x_1', defined so that $x_1' \equiv -\tau_1 U_c$ is an appropriate convection velocity of the large structure. A value of $0.65U_0$ was used for U_c, on

the basis of measurements presented in Antonia *et al.* (1983*b*). The origin $x_1' \equiv 0$ can be identified with $x_1 = 40d$, and positive and negative values of x_1' correspond respectively to locations downstream and upstream of the front. Identifying the maximum amplitude of $\langle\theta\rangle$ with the quantity a, the agreement between this value and that inferred from (9) is good over the complete range of x_2 (figure 8). The average frequency f_1, as obtained, from various methods, by Cervantes & Goldschmidt (1981) and Antonia *et al.* (1983*b*), is approximately $0.11U_0/L_u$. Equation (8) yields a value that is only 18% larger than this estimate. The crude ramp model in figure 8 is at best only a gross simplification, the ensemble averages in figure 9 providing some proof of this. Temperature ramps vary in shape and duration and, as noted by Mestayer (1982), they need not occur contiguously, tending at times to overlap and occasionally to disappear. Clearly the degree of organization and hence of these difficulties will vary from flow to flow. In spite of these drawbacks, it is difficult to ignore the good agreement (figure 8) between the ramp-model predictions and observations.

A more realistic attempt at modelling the ramp would be to use the measured conditional averages of $\langle\theta\rangle$. Such an approach was adopted by Subramanian & Antonia (1982); their calculations of $S_{\theta,1}$ were in reasonable agreement with measurements in a turbulent boundary layer. The approach followed below is essentially that of Subramanian & Antonia with one modification: it is simpler and sufficient to concentrate only on the sharp increase in $\langle\theta\rangle$ near $\tau_1 = 0$ or $x_1' = 0$, since the other parts of $\langle\theta\rangle$ make a negligible contribution to $S_{\theta,1}$.

With ensemble averaging defined by (10), the fluctuation β (note $\bar{\beta} = 0$) may be written as

$$\beta = \langle\beta\rangle + \beta^{\mathrm{r}}, \tag{11}$$

where $\langle\beta\rangle$ and β^{r} represent the coherent and random components of β. It follows from (11), after differentiating with respect to x_1, raising to the appropriate power and averaging, that

$$\overline{\beta_{,1}^2} = \overline{\langle\beta\rangle_{,1}^2} + \overline{(\beta_{,1}^{\mathrm{r}})^2}, \tag{12}$$

$$\overline{\beta_{,1}^3} = \overline{\langle\beta\rangle_{,1}^3} + \overline{(\beta_{,1}^{\mathrm{r}})^3}. \tag{13}$$

If $\beta_{,1}^{\mathrm{r}}$ is isotropic, $\overline{(\theta_{,1}^{\mathrm{r}})^3}$ and $\overline{(u_{2,1}^{\mathrm{r}})^3}$ should be negligible. If we first concentrate on temperature, (13) can be approximated by

$$\overline{\theta_{,1}^3} \approx \overline{\langle\theta\rangle_{,1}^3}. \tag{14}$$

In (12) and (13), correlations between coherent and random parts of $\beta_{,1}$ have been ignored. It is reasonable to assume that the major contribution from the coherent part is confined to the region (e.g. figure 9) associated with the sharp increase in $\langle\theta\rangle$ and that the rate of increase of $\langle\theta\rangle$ is constant. This rate is given by $a/(U_{\mathrm{c}}\tau_2)$, where τ_2 is the duration of this increase. The skewness $S_{\theta,1}$ can then be approximated by

$$S_{\theta,1} \approx \frac{(f_1\tau_2)^{-\frac{1}{2}}}{[1+\overline{(\theta_{,1}^{\mathrm{r}})^2}/\overline{\langle\theta\rangle_{,1}^2}]^{\frac{3}{2}}}. \tag{15}$$

An estimate of $\overline{(\theta_{,1}^{\mathrm{r}})^2}$ can be obtained from (12) using measured values of $\overline{\theta_{,1}^2}$ and $\overline{\langle\theta\rangle_{,1}^2}$. This latter quantity was determined by first differentiating the ensemble average with respect to x_1' (strictly with respect to time) and interpreting the overbar as an average over a distance $f_1^{-1}U_{\mathrm{c}}$. The quantity $[1+\overline{(\theta_{,1}^{\mathrm{r}})^2}/\overline{\langle\theta\rangle_{,1}^2}]$ varied between about 10 at $x_2 = 0$ to about 4 at $x_2 = L_u$; the inverse $\overline{\langle\theta\rangle_{,1}^2}/\overline{\theta_{,1}^2}$ of this ratio is shown in table 3. A direct estimate of $U_{\mathrm{c}}\tau_2$ can be made from figure 9. However, since the sudden increase in $\langle\theta\rangle$ is likely to be degraded by the jitter in arrival times of fronts, a more

x_2/L_u	$\overline{\langle u_1\rangle_{,1}^2}/\overline{u_{1,1}^2}$	$\overline{\langle u_2\rangle_{,1}^2}/\overline{u_{2,1}^2}$	$\overline{\langle\theta\rangle_{,1}^2}/\overline{\theta_{,1}^2}$	$\overline{\langle u_1\rangle_{,1}^3}/\overline{u_{1,1}^3}$	$\overline{\langle u_2\rangle_{,1}^3}/\overline{u_{2,1}^3}$	$\overline{\langle\theta\rangle_{,1}^3}/\overline{\theta_{,1}^3}$
0	1.5×10^{-2}	1.1×10^{-2}	0.11	6.5×10^{-3}	—†	0.46
0.17	1.6×10^{-2}	8.1×10^{-3}	0.09	6.2×10^{-3}	3.4×10^{-2}	0.28
0.33	1.6×10^{-2}	8.8×10^{-3}	0.11	7.2×10^{-3}	6.0×10^{-2}	0.36
0.5	2.1×10^{-2}	1.6×10^{-2}	0.16	1.1×10^{-2}	2.0×10^{-2}	0.44
0.67	1.7×10^{-2}	1.2×10^{-2}	0.14	1.0×10^{-2}	3.9×10^{-2}	0.36
0.83	2.0×10^{-2}	1.5×10^{-2}	0.21	1.5×10^{-2}	2.4×10^{-2}	0.55
1.0	2.2×10^{-2}	1.6×10^{-2}	0.24	1.4×10^{-2}	2.7×10^{-2}	0.59

† Note $\overline{u_{2,1}^3}$ is zero at $x_2/L_u = 0$.

TABLE 3. Estimates of contributions from coherent motion to $\overline{\beta_{,1}^2}$ and $\overline{\beta_{,1}^3}$

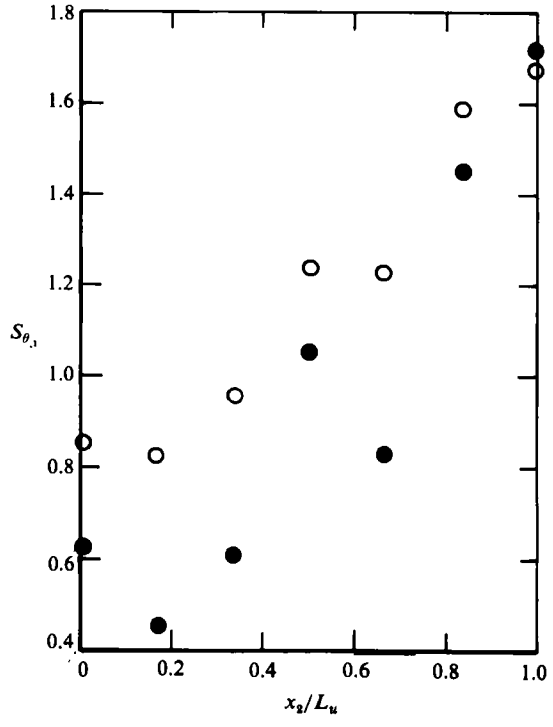

FIGURE 10. Comparison between measured and calculated skewness of the streamwise derivatives of temperature. Open and closed symbols respectively refer to measurement and calculation, equation (15).

appropriate estimate of $U_c\tau_2$ was obtained by first determining the maximum slope for each front, at or near $x_1' = 0$, and then averaging over the total number N of fronts. A similar procedure was used to obtain the average amplitude. Values of $\tau_2 U_0/L_u$ increased slightly from about 0.03 at $x_2 = 0$ to 0.04 at $x_2 = L_u$. The trend of $S_{\theta_{,1}}$ calculated with (15) correctly reflects the behaviour of the measurements (figure 10).

Relatively direct estimates of possible contributions of the large-scale coherent motion to $\overline{\beta_{,1}^2}$ and $\overline{\beta_{,1}^3}$ are given by the ratios of the first terms on the right sides of (12) and (13) to the corresponding terms on the left sides of these equations. These ratios, shown in table 3, indicate that the contribution from the coherent motion is negligible for velocity derivatives but important for temperature derivatives, especially $\overline{\theta_{,1}^3}$. The values indicated in the last column of table 3 only go about halfway

towards verifying (14) but, in view of the assumptions made in deriving (14) and the inevitable degradation of conditional averages with increasing distance from $x_1' \equiv 0$, the assumption that $\theta_{,1}^{\mathrm{r}}$ satisfies isotropy is not unreasonable. Whilst the contribution from the coherent motion to $\overline{u_{2,1}^3}$ is small, the skewness of $u_{2,1}$ is negligibly small, increasing slightly from zero at $x_2 = 0$ to about 0.1 at $x_2 = L_u$. Nonetheless, these results are consistent with the assumption that $u_{2,1}^{\mathrm{r}}$ satisfies isotropy. It is noteworthy that the contribution of the coherent motion to the skewness of $u_{1,1}$ is negligible. This result is of some importance since it leaves unaffected the observation, in §4, that the skewness of $u_{1,1}$ is reasonably approximated by the isotropic form of the vorticity budget. Van Atta (1977*b*) showed that the temperature-ramp model did not contribute to the correlation between the velocity-structure function and the squared temperature-structure function. This would leave unaffected the observation in §4 that the correlation between $u_{1,1}$ and $\theta_{,1}^2$ is correctly accounted for by the isotropic form of the temperature-dissipation budget.

6. Conditional averages of temperature dissipation

An attempt was made by Antonia *et al.* (1986) to delineate the topology of the large-scale motion in the present flow. Using measurements of $\langle u_1 \rangle$ and $\langle u_2 \rangle$ obtained with the rake [arrangement (iv), §2] at different values of x_2 and from a knowledge of the position of the front in the (x_1', x_2)-plane, streamline patterns associated with this motion were obtained, in the plane of main shear, with respect to an observer travelling with the convection velocity U_c of the motion. The emerging patterns showed up the presence of adjacent vortical structures on the same side of the centreline connected by a diverging separatrix, identifiable with the temperature front. These structures are asymmetric with respect to the centreline, the arrangement being in agreement with that suggested by Oler & Goldschmidt (1981) and Goldschmidt, Moalemmi & Oler (1983) on the basis of space–time correlations and smoke visualization in the self-preserving region of a plane jet.

Since the temperature front is associated with large streamwise gradients of velocity and especially temperature (figure 9) it would be natural to expect large values of $u_{1,1}^2$ and $\theta_{,1}^2$ to occur near the front. Apart from testing this expectation, an attempt is made in this section to map out the spatial distributions of $\theta_{,1}^2$, $\theta_{,3}^2$ and of an approximation to ϵ_θ, the instantaneous dissipation of $\frac{1}{2}\overline{\theta^2}$.

Signals proportional to $\theta_{,1}^2$, $\theta_{,3}^2$ and to an approximation of ϵ_θ were digitized with three other temperature signals from the spanwise rake [arrangement (iii), §2]. Not all the temperature signals of the rake could be digitized because of the maximum-sampling-frequency limitation (about 56 kHz) of the data-acquisition system. The sampling frequency used at each x_2 was in fact larger than twice the Kolmogorov frequency; the appropriate cut-off frequency for signals proportional to $\theta_{,1}^2$, $\theta_{,3}^2$ and ϵ_θ was determined by considering the signal-to-noise ratios of these quantities. The cutoff frequency which was used was larger than the Kolmogorov frequency by a factor in the range 1.3–2.6 depending on x_2. One of the three θ-signals that were digitized was the output from one of the parallel cold wires at the centre ($x_3 \approx 0$) of the rake while the other two were provided by wires located at $x_3 \approx \pm 0.3 L_u$. The approximation, here referred to as ϵ_θ for simplicity, to the instantaneous temperature dissipation, was constructed using a combination of $\theta_{,1}^2$ and $\theta_{,3}^2$ (the justification for and details of this construction are given in Anselmet & Antonia (1985)).

Observations of the three temperature traces displayed simultaneously with $\theta_{,1}^2$, $\theta_{,3}^2$ and ϵ_θ traces generally indicated good coincidence between the occurrence of fronts

and activity in $\theta^2_{,1}$, $\theta^2_{,3}$ or ϵ_θ. There was also, however, strong activity in these quantities immediately following the detection of a front. This was especially evident near $x_2/L_u = 1$. By contrast, the period preceding the detection showed relatively little activity. Periods of strong activity in $\theta^2_{,1}$, $\theta^2_{,3}$ and ϵ_θ also occurred when temperature fronts were absent, but this activity is unlikely to be spatially coherent. Similar observations were made by Jacquin (1983) on the basis of traces of θ and $\theta^2_{,1}$ obtained in a turbulent boundary layer at only one point in space.

To quantify the previous observations, conditional averages of $\theta^2_{,1}$, $\theta^2_{,3}$ and ϵ_θ were formed at every value of x_2, using (1). β now representing $\theta^2_{,1}$ or $\theta^2_{,3}$ or ϵ_θ. Resulting distributions at $x_2 = 0$ show (figure 11) that most of the activity is concentrated in a narrow region near $x_1' = 0$, the largest peaks occurring at negative values of x_1'/L_u. Conditional averages obtained at all values of x_2 were subsequently used to form contours of $\langle\theta^2_{,1}\rangle$, $\langle\theta^2_{,3}\rangle$ and $\langle\epsilon_\theta\rangle$ in the (x_1', x_2)-plane, using a procedure similar to that outlined at the beginning of this section. These three sets of contours were qualitatively similar, as might be inferred from figure 11, and therefore only $\langle\epsilon_\theta\rangle$ contours are shown in figure 12. Some smoothing was applied in figure 12, whereas the distributions in figure 11 were unsmoothed. The contours of $\langle\epsilon_\theta\rangle$ are clustered around the temperature front, which is indicated by the broken curve in figure 12. Approximate streamlines, as determined (Antonia *et al.* 1986) for an observer travelling downstream (right to left in figure 12) with a velocity U_c, have been added to figure 12 as an aid in locating the zone of large dissipation in relation to the coherent vortical structures. The largest values of $\langle\epsilon_\theta\rangle$ occur away from the centreline. Also, the contours are stretched towards larger negative values of x_1'/L_u near $x_2/L_u = 1$. Both these trends are consistent with the observation (Antonia *et al.* 1983*a*) that the largest values of the average production and dissipation of the temperature variance occur in this region of the flow.

The similarity between $\langle\theta^2_{,1}\rangle$ and $\langle\theta^2_{,3}\rangle$ in figure 11 might suggest that, with high probability, large temperature gradients, in the x_1 and x_3 directions, occur simultaneously. Such a trend would be at variance, however, with that displayed in figure 5 by the conventional j.p.d.f. of $\theta^2_{,1}$ and $\theta^2_{,2}$. It seemed therefore of some importance to investigate possible modifications to this trend by focusing only on zones of large dissipation. A conditional j.p.d.f. was obtained using only N portions of the digital record, each centred about the instant of detection of the front and extending over the range $-0.4 \leqslant x_1'/L_u \leqslant 0.4$. There is close similarity between conventional and conditional j.p.d.f. contours in figure 13, indicating that, even in the immediate vicinity of the front, large excursions of $\theta^2_{,1}$ and $\theta^2_{,3}$ do not, on average, occur simultaneously. On the contrary, large excursions of $\theta^2_{,1}$ occur, on average, when $\theta^2_{,3}$ is quiescent and *vice versa*.

It seems appropriate to comment on the likely three-dimensional configuration of zones of large dissipation. The present definition of the temperature front requires that temperature jumps are simultaneously detected over a distance, in the x_3 direction, of about L_u. Conditional averages of temperature, obtained over this distance, were identical, viz $\langle\theta\rangle_{,3} \equiv 0$, implying homogeneity in the x_3 direction, at least over a distance L_u. It seems reasonable to assume that there will be a large concentration of $\langle\theta^2_{,1}\rangle$ in the (x_1', x_3)-plane aligned with the direction of the front. In view of the limited evidence available, it would be difficult to infer with confidence the distribution of $\langle\theta^2_{,3}\rangle$ in the same plane. Speculatively, one possibility is that the region of large dissipation is a sheet of varying thickness which extends by an amount of order L_u in either the shear or spanwise directions and is aligned with the temperature front. We have noted that contours of the conditional rate of strain

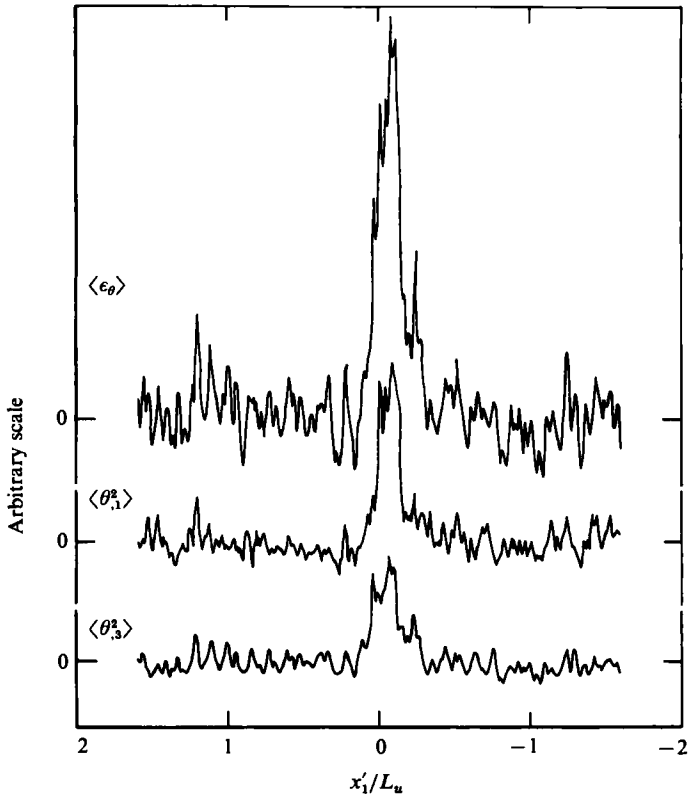

FIGURE 11. Conditional averages of $\theta^2_{,1}$, $\theta^2_{,3}$ and ϵ_θ at $x_2 = 0$.

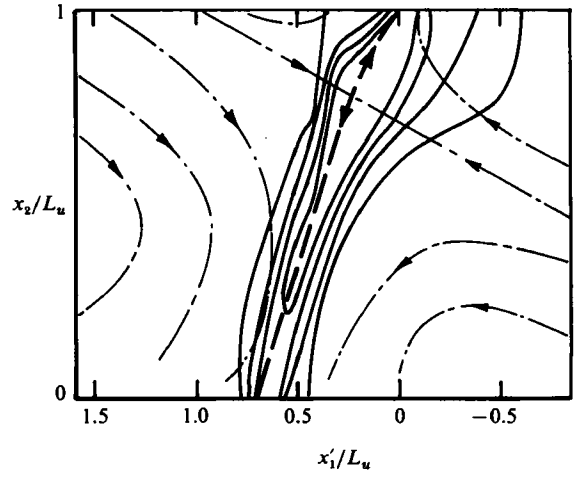

FIGURE 12. Contours of conditional averages of the temperature dissipation ϵ_θ. ——, outer-to-inner contours of $(\langle \epsilon_\theta \rangle L_u/U_0 T_0^2) \times 10^3$: 2.6, 5.2, 7.8, 10.4. The temperature front is indicated by the heavy broken line. — — —, approximate streamlines relative to an observer travelling from right to left with convection velocity of large structures.

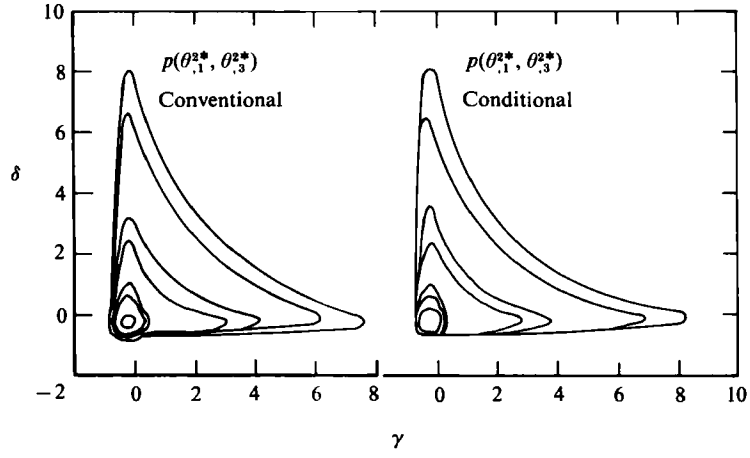

FIGURE 13. Conventional and conditional joint probability density functions between $\theta^2_{,1}$ and $\theta^2_{,3}$ at $x_2 = 0$. Magnitudes of outer-to-inner contours: 0.0005, 0.001, 0.005, 0.01, 0.05, 0.1, 0.5.

$(\langle u_1 \rangle_{,1} + \langle u_2 \rangle_{,2})$ have a large concentration in the direction of the front so that the high-dissipation zone should be approximately aligned with the direction of the principal rate of strain. The temperature front may be instantaneously curved or inclined to the x_3 direction so that large values of $\theta^2_{,1}$ and $\theta^2_{,3}$ need not occur simultaneously. Another, perhaps more likely, possibility is that zones of large dissipation are circular rods which are aligned, on average, with the direction of the front in the (x'_1, x_2)-plane. The cross-sectional dimensions of the rods, their spanwise spacing and their precise relationship with the front are matters that require further investigation. It is possible that a study along the lines outlined by Kuo & Corrsin (1972) may be useful in explicitly assessing the geometry of the fine structure. The ramp model used in the previous section represents, no doubt, a gross simplification of the physics. That it yields reasonable results for $S_{\theta,1}$ underlines the importance of the sudden change in temperature which is identifiable with the temperature front or the bounding surfaces of the large eddies. Although the assumed two-dimensionality of the ramp model receives partial support from observations of the front, the likely concentration of the dissipation in relatively narrow regions aligned with the front is not taken into account by the model.

7. Concluding comments

Various isotropy tests have been applied to data at moderate values of Reynolds and Péclet numbers. The isotropic forms of the vorticity and temperature-dissipation equations are satisfied approximately. Antonia *et al.* (1983*c*) found that, in the present flow, measured structure functions of velocity and temperature are in close agreement with isotropic calculations for these quantities over separations extending from the viscous to the inertial ranges. Reasonable agreement was found by Antonia *et al.* (1984, 1985) between measured spectra of velocity and temperature derivatives and calculations based on isotropy at sufficiently large wavenumbers. All the previous evidence suggests that both velocity and temperature fine-scale fields are isotropic. It would be clearly be useful to extend this conclusion to a wider range of turbulent Reynolds and Péclet numbers.

The non-zero skewness of the streamwise derivative of temperature and the non-zero

odd-order moments of the temperature structure function are apparently strong indicators of anisotropy. However, the measured odd-order temperature structure functions are consistent, in the context of local isotropy, with a crude ramp model of the temperature signature of the large-scale motion. The average amplitude and frequency of this signature are in good agreement with observations. A more realistic decomposition of temperature into anisotropic coherent and isotropic random components leads to an encouraging agreement between calculation and measurement of the temperature-derivative skewness. When the coherent component is mathematically identified with conditional averages obtained from information at several points in space, this component is shown to make a significant contribution to the skewness of the temperature derivative but a negligible contribution to the velocity-derivative skewness. The last two results are consistent with local isotropy.

Isotropic relations between mean-square derivatives with respect to different spatial directions are satisfied by neither temperature nor velocity. To our knowledge, there is no firm indication that this departure from isotropy decreases with increasing Reynolds number. It is important that this departure is taken into account both experimentally and in computational models. A likely source of this anisotropy may be the major contribution to derivatives in either lateral or spanwise directions from the relatively small wavenumber range of the spectrum.

Conditional averages of squared derivatives of temperature in the streamwise and spanwise directions indicate relatively high amplitudes in a relatively narrow region immediately following the detection of the temperature front. There is therefore a large concentration of temperature dissipation which is approximately aligned with the temperature front in the direction of the principal rate of strain. The characteristic dimensions of this zone are not known precisely but we speculate that this zone extends much more significantly along the front than in either the streamwise or spanwise directions.

The authors are grateful to Drs L. W. B. Browne and D. H. Britz for their contributions to the experimental and computational aspects of the work. F.A. acknowledges the Australian–European Awards Program which supported his visit to the University of Newcastle. The support of the Australian Research Grants Scheme is gratefully acknowledged.

REFERENCES

ANSELMET, F. 1983 Intermittence Interne de la Turbulence Pleinement Développée: Calcul de Fonctions de Structure d'Ordres Elevés et Applications à la Combustion. Thèse Docteur Ingénieur, Institut National Polytechnique de Grenoble.

ANSELMET, F. & ANTONIA, R. A. 1985 *Phys. Fluids* **28**, 1048–1054.

ANTONIA, R. A. & BROWNE, L. W. B. 1983 *J. Fluid Mech.* **134**, 67–83.

ANTONIA, R. A., BROWNE, L. W. B. & CHAMBERS, A. J. 1984 *Phys. Fluids* **27**, 2628–2631.

ANTONIA, R. A., BROWNE, L. W. B. & CHAMBERS, A. J. 1985 *Phys. Fluids* **28**, 420–423.

ANTONIA, R. A., BROWNE, L. W. B., CHAMBERS, A. J. & RAJAGOPALAN, S. 1983*a* *Intl J. Heat Mass Transfer* **26**, 41–48.

ANTONIA, R. A., BROWNE, L. W. B., RAJAGOPALAN, S. & CHAMBERS, A. J. 1983*b* *J. Fluid Mech.* **134**, 49–66.

ANTONIA, R. A., CHAMBERS, A. J., BRITZ, D. & BROWNE, L. W. B. 1986 *J. Fluid Mech.* [submitted].

ANTONIA, R. A., CHAMBERS, A. J. & BROWNE, L. W. B. 1983*c* *Expts in Fluids* **1**, 213–219.

ANTONIA, R. A., PHAN-THIEN, N. & CHAMBERS, A. J. 1980 *J. Fluid Mech.* **100**, 193–208.

ANTONIA, R. A., SATYAPRAKASH, B. R. & HUSSAIN, A. K. M. F. 1982 *J. Fluid Mech.* **119**, 55–89.

ANTONIA, R. A. & VAN ATTA, C. W. 1978 *J. Fluid Mech.* **84**, 561–580.

BATCHELOR, G. K. & TOWNSEND, A. A. 1947 *Proc. R. Soc. Lond.* A **190**, 534–550.

BRADSHAW, P. 1967 *Aero. Rep.* 1220 ARC28664 FM3798, National Physical Laboratory, London.

BRADSHAW, P. 1969 *Rep.* RM3603, Ministry of Technology Aeronautical Research Council, London.

BROWNE, L. W. B., ANTONIA, R. A. & CHAMBERS, A. J. 1983*b* *Boundary-Layer Met.* **27**, 129–140.

BROWNE, L. W. B., ANTONIA, R. A. & RAJAGOPALAN, S. 1983*a* *J. Phys. Fluids* **26**, 1222–1227.

BUDWIG, R., TAVOULARIS, S. & CORRSIN, S. 1985 *J. Fluid Mech.* **153**, 441–460.

CERVANTES DE GORTARI, J. & GOLDSCHMIDT, V. W. 1981 *Trans. ASME* I: *J. Fluids Engng* **103**, 119–126.

CHAMPAGNE, F. H. 1978 *J. Fluid Mech.* **86**, 67–108.

CHAMPAGNE, F. H., FRIEHE, C. A., LARUE, J. C. & WYNGAARD, J. C. 1977 *J. Atmos. Sci.* **34**, 515–530.

CHAMPAGNE, F. H., HARRIS, V. G. & CORRSIN, S. 1970 *J. Fluid Mech.* **41**, 81–139.

CORRSIN, S. 1963 *Handbuch der Physik VIII/2* (ed. S. Flugge & C. Truesdell), pp. 524–590. Springer.

EVERITT, K. W. & ROBINS, A. G. 1978 *J. Fluid Mech.* **88**, 563–583.

FRENKIEL, F. N. & KLEBANOFF, P. S. 1975 *Boundary-Layer Met.* **8**, 173–200.

FULACHIER, L. & ANTONIA, R. A. 1983 *Intl Comm. Heat Mass Transfer* **10**, 435–439.

GAGNE, Y. & HOPFINGER, E. J. 1979 In *Proc. 2nd Intl Turbulent Shear Flows Conference, Imperial College, London, 11.7–11.12.*

GIBSON, C. H., FRIEHE, C. A. & MCCONNELL, S. 1977 *Phys. Fluids* **29**, S156.

GOLDSCHMIDT, V. W., MOALLEMI, M. K. & OLER, J. W. 1983 *Phys. Fluids* **26**, 428–432.

GUTMARK, E. & WYGNANSKI, I. 1976 *J. Fluid Mech.* **73**, 465–495.

HARRIS, V. G., GRAHAM, J. A. H. & CORRSIN, S. 1977 *J. Fluid Mech.* **81**, 657–687.

HESKESTAD, G. 1965 *Trans. ASME* E: *J. Appl. Mech.* **87**, 735.

JACQUIN, L. 1983 Etude de Comportement Intermittent de la Dissipation dans une Couche Limite à Grand Nombre de Reynolds. Thèse Docteur 3eme Cycle, Université d'Aix-Marseille II.

KERR, R. M. 1985 *J. Fluid Mech.* **153**, 31–58.

KOLMOGOROV, A. N. 1941*a* *C.R. Akad. Sci. USSR* **30**, 301–305.

KOLMOGOROV, A. N. 1941*b* *Dokl. Akad. Nauk SSSR* **32**, 19–21.

KUO, A. Y-S. & CORRSIN, S. 1971 *J. Fluid Mech.* **50**, 285–320.

KUO, A. Y-S. & CORRSIN, S. 1972 *J. Fluid Mech.* **56**, 447–479.

LAWN, C. J. 1971 *J. Fluid Mech.* **48**, 477–505.

LUMLEY, J. L. 1965 *Phys. Fluids* **8**, 1056–1062.

MESTAYER, P. 1982 *J. Fluid Mech.* **125**, 475–503.

MESTAYER, P. & CHAMBAUD, P. 1979 *Boundary-Layer Met.* **16**, 311–329.

MESTAYER, P., CHOLLET, J. P. & LESIEUR, M. 1984 *Turbulence and Chaotic Phenomena in Fluids* (ed. T. Tatsumi), pp. 285–288. North-Holland.

MONIN, A. S. & YAGLOM, A. M. 1975 *Statistical Fluid Mechanics: Mechanics of Turbulence, Vol. II.* MIT Press.

NELKIN, M. & NAKANO, T. 1984 *Turbulence and Chaotic Phenomena in Fluids* (ed. T. Tatsumi), pp. 319–323. North-Holland.

OLER, J. W. & GOLDSCHMIDT, V. W. 1981 In *Proc. 3rd Symp. on Turbulent Shear Flows, Davis, 11.1–11.4.*

PARANTHOEN, P., PETIT, C. & LECORDIER, J. C. 1982 *J. Fluid Mech.* **124**, 457–473.

SCHEDVIN, J., STEGEN, G. R. & GIBSON, C. H. 1974 *J. Fluid Mech.* **65**, 561–579.

SREENIVASAN, K. R., ANTONIA, R. A. & BRITZ, D. 1979 *J. Fluid Mech.* **94**, 745–775.

SREENIVASAN, K. R., ANTONIA, R. A. & DANH, H. Q. 1977 *Phys. Fluids* **20**, 1238–1249.

SREENIVASAN, K. R. & TAVOULARIS, S. 1980 *J. Fluid Mech.* **101**, 783–795.

SUBRAMANIAN, C. S. & ANTONIA, R. A. 1982 *Phys. Fluids* **25**, 957–958.

TAVOULARIS, S. & CORRSIN, S. 1981 *J. Fluid Mech.* **104**, 349–367.

TAYLOR, R. J. 1958 *Austral. J. Phys.* **11**, 168–176.

TENNEKES, H. & WYNGAARD, J. C. 1972 *J. Fluid Mech.* **55**, 93–103.

VAN ATTA, C. W. 1977*a* *J. Fluid Mech.* **80**, 609–615.

VAN ATTA, C. W. 1977*b* *Arch. Mech.* **29**, 161–171.

VEROLLET, E. 1977 Etude d'une Couche Limite Turbulente avec Aspiration et Chauffage à la Paroi. Ph.D. Thesis, I.M.S.T., Marseille (*Rapport CEA*-R-4872, C.E.N. Saclay).

WYGNANSKI, I. & FIEDLER, H. 1969 *J. Fluid Mech.* **38**, 577–612.

WYNGAARD, J. C. 1968 *J. Sci. Instrum.* **1**, 1105–1108.

WYNGAARD, J. C. 1969 *J. Sci. Instrum.* **2**, 983–987.

WYNGAARD, J. C. 1971*a* *Phys. Fluids* **14**, 2052.

WYNGAARD, J. C. 1971*b* *J. Fluid Mech.* **48**, 763–769.

WYNGAARD, J. C. & CLIFFORD, S. F. 1977 *J. Atmos. Sci.* **34**, 922–929.

WYNGAARD, J. C. & TENNEKES, H. 1970 *Phys. Fluids* **13**, 1962–1969.

YAGLOM, A. M. 1949 *Dokl. Akad. Nauk SSSR* **69**, 743–746.

YAGLOM, A. M. 1981 *Izv. Atmos. Ocean. Phys.* **17**, 919–935.